BILINGUAL PUBLISHING GROUP
Pioneer of Global Academics Since 1984

Advances in Geological and Geotechnical Engineering Research
https://journals.bilpubgroup.com/index.php/agger

ARTICLE

Petrogenesis and Rb-Sr Isotopic Characteristics of Paleo-Mesoproterozoic Mirgarani Granite Sonbhadra Uttar Pradesh India: Geodynamics Implication for Supercontinent Cycle

***A.P. Dhurandhar*[1*], *Suresh Khirwal*[2], *D.V.L.N. Sastry*[3]**

[1] *Orion Geohytech India, G-10 Bramhaputra Apartment, Aakar Nagar, Katol Road, Nagpur, 440013, India*
[2] *Atomic Minerals Directorate for Exploration & Research, Jamshedpur, 831014, India*
[3] *Atomic Minerals Directorate for Exploration & Research, Hyderabad, 009140, India*

ABSTRACT

The Rb-Sr whole-rock isochron, age 1636 ± 66 Ma of Mirgarani granite, is the one of the oldest granite dated in the northwestern part of the Chhotanagpur Granite Gneiss Complex (CGGC). The initial Sr ratio is 0.715 ± 0.012 (MSWD = 0.11), showing an S-type affinity. The Mirgarani granite has intruded the migmatite complex of the Dudhi Group and forms the Mirgarani formation comparable to the granites of the Bihar Mica Belt around Hazaribagh (1590 ± 30 Ma). The present studies have established the chronostratigraphy of the Dudhi Group and adjoining areas in CGGC. Petrographic and geochemical studies revealed that the granite is enriched in Rb (271 ppm), Pb (77 ppm), Th (25 ppm), and U (33 ppm) and depleted in Sr (95 ppm), Nb (16 ppm), Ba (399 ppm) and Zr (143 ppm) contents as compared to the normal granite. The Mirgarani granite is a peraluminous (A/CNK = 1.23), high potassic (K_2O 6.42%), Calc-Alkalic to Alkali-Calcic {(Na_2O + K_2O) - CaO = 6.29} S-Type granite, a feature supported by the presence of modal garnet and normative corundum (2.68%). The Mirgarani granite is considered to have been formed by the anatexis of a crustal sedimentary protolith at a depth of approximately 30 km with temperatures ranging from 685-700 °C during the Columbian - Nuna Supercontinent.

Keywords: Miragrani granite; Petrogenesis; Isochron dating; Radiogenic heat; Dudhi group; CGGC; Palaeo-Mesoproterozoic; Supercontinents

*CORRESPONDING AUTHOR:
A.P. Dhurandhar, Orion Geohytech India, G-10 Bramhaputra Apartment, Aakar Nagar, Katol Road, Nagpur, 440013, India; Email: apdhurandhar@gmail.com

ARTICLE INFO
Received: 17 November 2022 | Revised: 15 January 2023 | Accepted: 29 January 2023 | Published Online: 21 February 2023
DOI: https://doi.org/10.30564/agger.v5i1.5261

CITATION
Dhurandhar, A.P., Khirwal, S., Sastry, D.V.L.N., 2023. Petrogenesis and Rb-Sr Isotopic Characteristics of Paleo-Mesoproterozoic Mirgarani Granite Sonbhadra Uttar Pradesh India: Geodynamics Implication for Supercontinent Cycle. Advances in Geological and Geotechnical Engineering Research. 6(1): 57-86. DOI: https://doi.org/10.30564/agger.v5i1.5261

1. Introduction

The northwestern part of Chhotanagpur Granite Gneiss Compex (CGGC) occurs in the Sonbhadra district of Uttar Pradesh (U.P.) and, the Mahakoshal group of rock occurs in the north of the CGGC and, is separated by Son Narmada South fault (SNSF). The systematic geological mapping of the rocks of the Son valley and northwestern part of CGGC in the Sonbhadra district of U.P. has been rather scanty and also a cogent account of chrono-stratigraphy is not available. This part of CGGC was named Dudhi Group by Dayal [1], who gave the first geological succession of the Mirzapur and Sonbhadra area. Subsequently, the regional stratigraphic succession based on photo-characteristics was given by Iqubal-luddin and Moghani [2]. The rocks of the Son valley area have been mapped as the Son Valley greenstone belt by Chaubey and Gupta [3]. The Son Valley rocks have been considered distinct and older than the Bijawars of the type of area and designated as the Mahakoshal Group [4]. The rock formations the south of the Son-Narmada South fault, locally known as the Dudhi Fault, is designated as the Dudhi Group and correlated with the Chhotanagpur Granite Gneiss Complex (CGGC) of Bihar by Yadav [5]. Later, a detailed geological succession for the north and south of the rift valley, along with the account of uranium mineralization in the area, was given by Bhattacharya et al. [6].

The CGGC is an east-west trending mobile belt that belongs to the east Indian Shield and is exposed across the states of Jharkhand, Bihar, West Bengal, and Chhattisgarh, covering an area of over 100,000 km^2 [7,8]. The northern margin of the CGGC is covered by quaternary sediments of Gangetic alluvium (**Figure 1**). Sediments of the Bengal Basin mark the eastern boundary of the terrain and the Mesozoic volcanic of Rajmahal Trap covers the northeastern fringe of the terrain. The western margin of CGGC is dominantly covered by Gondwana deposits of Permian to mid-Cretaceous age [7]. The Mirgarani granite occurs in the northwestern part of the CGGC occurs across the Rihand valley district Sonbhadra (U.P.) and hosts several uranium occurrences. The regional folding and tectonics of CGGC were given based on regional structural and petrographic studies from the central and eastern parts of the Chhotanagpur terrain. Sarkar [9-11] suggested a tentative temporal relationship between the three phases of structural deformation, metamorphism and granite emplacement. Based on reviews of petrological, geochemical, metamorphic, deformational, and geochronological data on the CGGC given as summarised as [12-15]:

M_1 metamorphic stage (around 1870 Ma and followed by the D_1 deformation, > 900 °C at 5-8 kbar pressure).

M_2 metamorphic phase between 1660 Ma and 1270 Ma, the D_2 deformation, 700-800 °C at 5-7 kbar pressure).

M_3 phase was recorded between 1200 Ma and 930 Ma, 700 ± 50 °C at 6.5±1 kbar pressure followed by a D_3-Grenvillian Orogeny.

M_4 event at 870-780 Ma around 750-600 °C and 9-12 kbars pressure, and D_4 and D_5 deformation; D_6 deformation around 850-800 to 600 Ma final cooling.

Mukherjee et al. [16] have divided CGGC into three major tectonostratigraphic classes Domain I, II, and III; Domain I is further divided into two geographic sub-domains viz. Domain IA (south) and IB (north) (**Figure 1a**). These are all based on the geochronological data from the central and eastern parts of CGGC and geomorphic features but they are not based on any tectonic lineament, etc. Present study area and adjoining parts very limited granites/granitoids have been studied so far namely around Harnakachar, Katoli granitoid, Dudhi Granite, Raspahari in CGGC, and In Mahakoshals Tumiya, Jhirgadandi granitoid, and Neruiyadamar granitoids. The present paper discusses new Rb-Sr isotopic data and petrogenesis of Mirgarani granite, regional chronostratigraphy of the area, and provides its implications in the Chhotanagpur granite gneiss complex (CGGC) by synthesizing Rb-Sr isotopic data from the western and northwestern part of CGGC.

2. Regional geology

The Son Valley greenstone belt (Mahakoshal Group) is bounded by the rocks of the Vindhyan

Supergroup in the north and south by the Dudhi and Gondwana group rocks. The northern contact along the Vindhyan is marked by a fault that is an extension of the Jamual-Markundi Fault [17] or the Great Boundary Fault [18]. The Jhirgadandi granite is emplaced along this northern fault in the phyllites of the Turbidite Group (**Figure 1b**). The southern contact of the Son Valley group of rocks (Mahakoshal Group) with the migmatites, granite gneisses, metasediments of the Dudhi group, and rocks of the Gondwana sequence are also faulted and is known as the Dudhi Fault or Son-Narmada South Fault. This contact has several intrusive granitic bodies, namely the Windhyamganj, Harnakachar, Katoli, Bagishoti, Neruiyadamar Granitoid, Tumiya Granitoid, alkali feldspar granite, and alkali epi-syenites of the Sonwani and Kundabhati areas (7, K, S in **Figure 1b**). The regional strike of the Mahakoshal Group greenstone belt is ENE-WSW, with steep dips towards the south. The presence of mesoscopic folds, faults, fractures, crenulations, and puckers of varying trends in Bijawar indicate that these formations were subjected to deformational forces over a considerable period, which caused repeated folds and faults. The Bijawar formations display tight isoclinal to overturned folds plunging at low to moderate angles towards the east and west; these appear to have been developed in the first phase of deformation, which was probably the most active. The subsequent phases of deformation were responsible for the development of subsidiary folds superposed on the first generation of folds [19]. The Mahakoshal Group has been transected by several fractures trending along and across formation trends. Faults trending ENE-WSW and E-W along the Son River north of Renusagar affect the Mahakoshal Group, Dudhi group, and Gondwana. The N-S trending faults have been recorded along the Rihand River. The trend of the Vindhyan Formation varies from NE-SW to ENE-WSW but dips at a low angle towards the north. The Gondwana occurs in a faulted basin. The major tributaries of the Son River and a few major streams follow a straight course with N-S, NW-SE, and NE-SW trends that reflect the underlying fracture trends (**Figure 1b**).

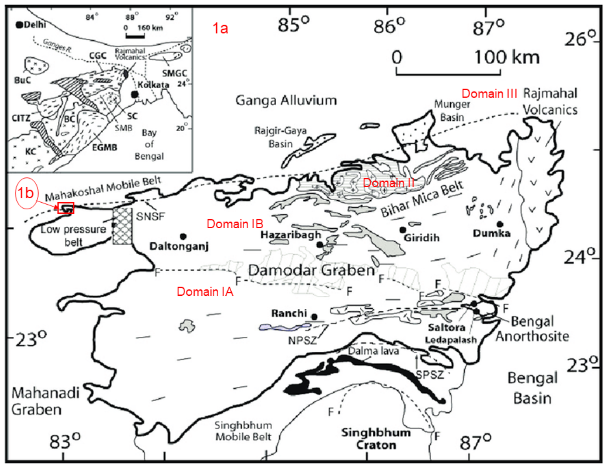

Figure 1a. Regional map showing the Chhotanagapur Granite Gneiss complex and inset India map.

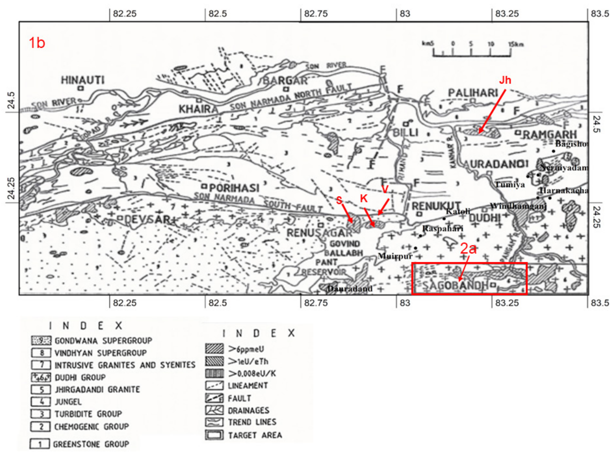

Figure 1b. Regional map of Sonbhadra District showing Mahakoshal and Northwestern part of CGGC, S: Sonwani, K: Kundabhati, V: Vikasnagar; Jh: Jhirgadandi.

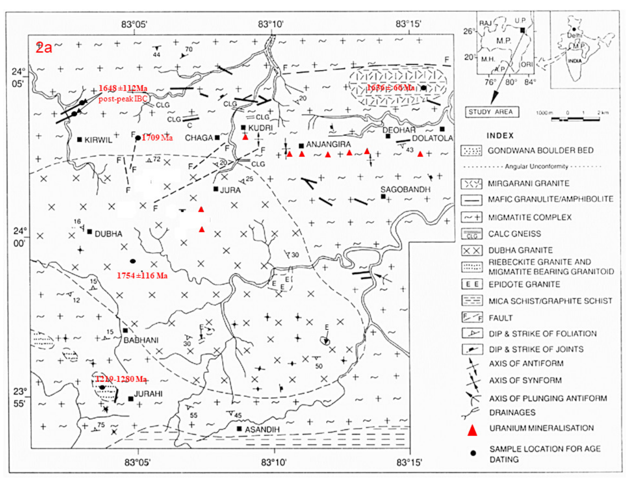

Figure 2a. Geological map of Dudhi Group Sonbhadra District U.P. modified after Dayal 1979 [1].

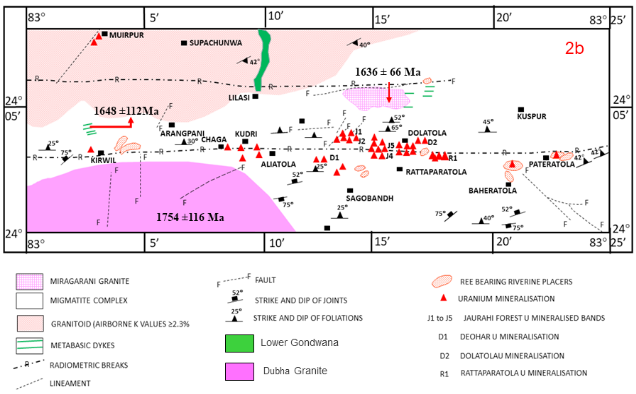

Figure 2b. Detailed geological map of the area around Mirgarani Granite showing uranium occurrences.

3. Geology of the study area

The Mirgarani granite is a high hillock elongated in the E-W direction, forms a domal outcrop in the surrounding low-lying migmatite country rock, and supports a radial drainage pattern. It shows cross-cutting relationships with the meta-basics (amphibolite dykes, calc-granulite, and variants of the migmatite complex), thereby showing intrusive relationships with the migmatite complex (**Figures 2a and 2b**) of the Dudhi Group. Three sets of lineaments were observed: NE-SW, ENE-WSW, and east-west. The migmatite complex hosts several uranium occurrences in Anjangira-Deohar and north of Sagobandh village (**Figure 2a**) [20-23]. The Dudhi Group unconformably overlies the Archean basement and starts with transition sediments with oligomictic quartz pebble meta conglomerates overlaid by Metamorphites, Migmatite Complex, and younger intrusive granites, of various ages Mafic Granulites, and syenites. The migmatite complex consists of palaeosols, mesosomes, biotite melanosomes, stromatic migmatite, pegmatoid, granitoid leucotomies, concordant and discordant bodies of amphibolites, mafic granulites with bands calc-silicate rocks and colonies. Besides these, the mappable variants of granite present in the area are the biotite-hornblende granite of Dubha, magnetite-bearing granitoid, and riebeckite granite of Jaurahi, steno-granites of Mirgarani hillock, and a few outcrops of epidote granite. The mica schist and graphite schist crops south of Asandih (**Figure 2a**). The youngest rocks in the area are Lower Gondwana Sediments with Faulted/unconformity contacts with the Dudhi group of rocks. The area has undergone medium to high-grade regional metamorphism reaching up to upper amphibolite to granulite grade, and a large part of the area belongs to sillimanite—orthoclase isograd. The chronostratigraphic succession of the area is provided in **Table 1**.

Petrography

The Mirgarani granite is leucocratic fine-to medium-grained greyish and pinkish. Under the microscope, it shows a hypidiomorphic granular texture with myrmekitic growth. In some places, it exhibits gneissosity due to parallel alignments of biotite flacks. The essential minerals are potash feldspars (orthoclase, string perthite), quartz, and plagioclase feldspars of albite-oligoclase composition. Biotite and garnet are the chief accessory minerals with minor zircon, apatite, and opaque minerals, such as Ti-magnetite and ilmenite. Medium-sized porphyroblasts of potash feldspars containing inclusions of rounded quartz, albite-oligoclase feldspars, myrmakites, and biotite are suggestive of potash metasomatism. Pink-colored pyrope-almandine garnet was formed at the expense of biotite. The bending of biotite flakes and plagioclase lamellae and the fracturing of quartz and garnet indicate mild stress effects. Mineralogical alterations are of very low intensity and include a slightly cloudy appearance in plagioclase feldspars, saussiritisation in plagioclase feldspar, dendritic growth in biotite, and occasional martitisation in magnetite. Volumetric percentages of modal mineralogy (**Table 2**) and their plots in the QAP diagram of Streckeissens [25] classify Mirgarani granite as Syeno-granites; only three samples fall in the Alkali feldspar granite field (**Figure 3**).

Table 1. Chronostratigraphy of Dudhi Group.

Period	**Group**	**Formation**	**Lithology**
Recent			Alluvium
Permo-Carboniferous (Lower Gondwana)			Lower Gondwana Sediments
~~Fault /Unconformity~~~~~~~~~~~~~~~~~~~~~~~~~~~~			
Neoproterozoic			Syenites (900 Ma) Alkali feldspar granite Sonwani and Kundabhati (1292 Ma) [97]
Mesoproterozoic 1400-1600 Ma	Dudhi	Intrusive Granites	Tourmaline granite Leucogranite garnetiferous granite and Riebeckite Granites of the Jaurahi Area (1219-1280 Ma) [74]
			Dudhi Granite 1576 ± 76 Ma [75]
Palaeoproterozoic>1600 Ma			Mirgarani Granite 1636 ± 66 Ma
			Kirwil-Sagobabdh Mafic Granulite 1648 ± 112 Ma (post-peak isobaric cooling) [23]
			Harnakachar granitoid 1710 Ma [81]
			Vikasnagar Granite 1717 Ma, [97]
			Rihand Granite 1731 ± 36 Ma
			Katoli granitoid 1730 Ma [81]
			Raspahari Granitoid ca. 1750 Ma [81]
			Dubha Granite 1754 ± 116 Ma [22]
			Muirpur Granite Gniesses 1709 ± 102 Ma [75]
		Migmatite Complex 1787 ± 72 Ma [24]	Quartz Veins
			Quartz Microclene Viens
			Pegmatoid Leucosome Mobilizates (PLM)
			Granitoid Leucosome Mobilizates (GLM)
			Biotite Melanosomes
			Migmatite Mobilizate complex Palaeosomes and Mesosomes (PS, MS)
			Metamorphosed and Ultrametamorphosed Transition Sediments (TS)
		Metamorphites	Metamorphosed and Ultrametamorphosed Transition Sediments (TS)
~~Unconformity~~~~~~~~~~~~~~~~~~~~~~~~~~~~~~			
			Transition Sediments with Oligomictic quartz pebble meta-conglomerates (Dauradand area)
~~Fault / Unconformity~~~~~~~~~~~~~~~~~~~~~~~~~~~~			
Archean ~2600 Ma			Augen gneiss, porphyritic granite, granite gneiss, Amphibolites, banded ferruginous quartzite, Hornblende schist, dolomites, graphite schists, pyroxene granulite, leptinites, and calc-silicate rocks.

Modified after Dhurandhar and Saxena (1996) [20].

Table 2. Modal mineralogy on Mirgarani granite.

Minerals	MR/1	MR/2	MR/3	MR/4	MR/5	MR/6	MR/7	MR/8
K-Feldspar	49.2	53.4	46.6	53.7	45.4	50.7	53.1	58.4
Ab-Oligoclase	10.2	11.6	7.7	18.3	18.3	7.0	8.4	9.7
Quartz	35.2	27.4	33.7	20.8	22.1	30.9	33	25.4
Biotite	2.4	4.7	1.6	3.8	4.7	10.4	4.3	4.5
Garnet	2.4	2.1	9.3	3	2.8	0.4	0.8	1.5
Opaques	0.2	0.6	1	0.3	0.6			
Others	0.4	0.1	0.1	0.1	0.5	0.3	0.1	0.1

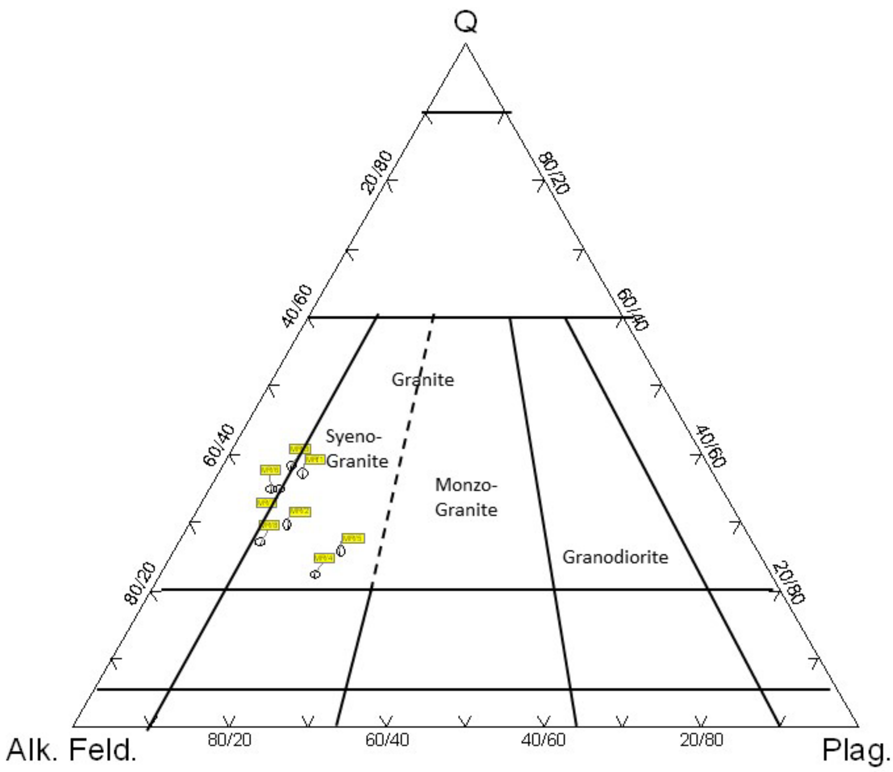

Figure 3. Modal QAP Diagram after Strieckesens (1976) [25] for Mirgarani Granite. Fields 0 Quartzolite, 1 Quartz rich Granitoid, 2 Alkali Feldspar Granite, 3 Granite, 4 Granodiorite, 5 Tonalite, 6 Quartz alkali feldspar Syenite, 7 Quartz Syenite, 8 Quartz Monzonite, 9 Monzodiaorite Monzogabbro, 10 Quartz Diorite Quartz Gabbro, Quartz Anorthosite, 11 Alkali Feldsapr Syenite, 12 Syenite, 13 Monzonite, 14 Foid bearing Monzo diorite monzo gabbro, 15 Diorite, Gabbro Anorthosite.

4. Sampling and analytical techniques

The bulk samples were cleaned, broken, and crushed using a jaw crusher. After quartering and coning, a representative sample was ground to -200 mesh in a shatter box for whole-rock isotopic analysis. One set of samples was analyzed for major, minor, and trace elements by the wavelength dispersive X-ray fluorescence method using international standards as reference USGS, INRT IGI, RIAP, namely: G1, G2, GSP1, GS-N, SG-1a, SG2, and SG3. The accuracy of the analysis of relative analytical uncertainties is as follows: Si, Al (< 1%), Fe, Mg, Ca (1%-2%), Ti, Na, K (3%-5%), P, and other trace elements (£ 6%). The samples were digested using concentrated HF and HNO_3 in Teflon digestion bombs at 130 °C for 48 h. This was followed by dissolution in HCl acid (HCl). Separation of Rb and Sr from dissolved rock solutions was carried out by ion-exchange chromatography using an AG 50WX12 cation exchange resin in a clean lab under laminar flow. Quantitative estimation of these elements was performed by spiking a known amount of a mixed ^{87}Rb-^{84}Sr tracer, before decomposition. The Rb and Sr isotopic compositions were analyzed using conventional mass spectrometric isotopic dilution techniques with a fully automated, multi-collector thermal ionization mass spectrometer model VG-354. Rb and Sr were loaded as chloride and nitrate, respectively, on Ta ribbon single filament beads with a 1 μL drop of 1N H_3PO_4. The ^{87}Rb and ^{87}Sr tracers used to determine Rb and Sr were calibrated against gravimetrically prepared J. M. salts. Appropriate fractionation corrections were applied to improve accuracy. Based on the replicate analysis, the errors at the 2σ level were 2% for $^{87}Rb/^{86}Sr$ and 0.05% for $^{87}Sr/^{86}Sr$. The mean value for ($^{87}Sr/^{86}Sr$) ratio of the SRM-987 standard was 0.710241 ± 23 (N = 15). Excel plugin Isoplot 3.7 software [26] was used to calculate the slope and intercept of the isochrons. The errors in age and initial Sr ratios quoted here are two standard deviations. More information on the age-dating analytical processes can be found elsewhere [27].

5. Geochemistry

The chemical composition of the Mirgarani granite is presented in **Table 3**. In general, Mirgarani granite shows SiO_2 67.39%-71.9%, TiO_2 0.12 to 0.43%, Al_2O_3 13.46%-14.32%, CaO 1.15%-1.6%, MgO 0.12%-0.36%, FeO 0.97%-1.91%, Fe_2O_3 0.97%-1.91%, MnO 0.03%-0.05%, K_2O 6.02%-6.96%, Na_2O 0.75% to 1.53% and P_2O_5 0.06%. LI 25.29-26.97, DI 75.44-85.74, and FI vary from 83.93-86.99. The Mirgarani granite is enriched in K_2O, FeO, Rb (271 ppm), Pb (77 ppm), Th (25 ppm), U (33 ppm), Cr (27 ppm), Ni (26 ppm), and Co (8 ppm) and depleted in Sr (95), Nb (16 ppm), Ba (399 ppm), and Zr (143 ppm) as compared to the normal granite [28] and continental crust [29]. SiO_2 showed a positive correlation with Al_2O_3, Na_2O, CaO, Larsen's index (LI), Cr, Ni, Ge, As, Sr, Pb, Th, and U and negative correlations with TiO_2, FeO (T), MgO, MnO, K_2O, DI, FI, Rb, Zr, and Nb. On chondrite-normalized multi-element plots (**Figure 4a**), the Mirgarani granite show relative enrichments in Rb, Ba, Th, U, K, Nb, Ce, Sr, Zr, and, with pronounced negative P, and Ti anomalies [30]. The same patterns are shown in primitive mantle normalized plots showing depletion in P and Ti and enrichment in all other elements (**Figure 4b**) [31]. Their multi-element patterns are quite similar to S-Type plutons, although the elemental abundances are variable over a large range from 1.1 to hundreds of times the normalizing values and, likely reflecting source heterogeneities. The Mirgarani granite is peraluminous with A/CNK = 1.17 – 1.31 (average 1.23) and A/NK varies from 1.53 to 1.66 with an average of 1.58 (**Figure 5a**) Shand's index diagram [32]. Agpaitic Index (AI) varies from 0.60 to 0.66 with an average of 0.64. Mirgarani granite is high potassic (K_2O = 6.42%) and has high silica (SiO_2 70.69% avg.), Low Calcic (CaO 1.33 avg.), and magnesium #Mg. 4.22 (**Table 3**) and bearing S-type alkali granite (**Figure 5b**). The S-type feature is further supported by the presence of modal garnet normative corundum 2.52% (**Table 3**) and also by the ACF diagram (**Figure 5c**), where all samples plot in the S-type field. Mirgarani Granites have Low Na_2O content (1.15% avg.), CaO (1.33% avg.), and Sr (95 ppm avg.) contents, which are lost during the conversion of feldspar to clay minerals by weathering and are therefore low in pelitic rocks. Sodium was removed from the solution along with Ca, Sr, and Pb. The Mirgarani Granite also has high Ni, Co, and Cr contents.

Table 3. Geochemical data on Mirgarani Granite showing Major oxides in wt%, trace elements in ppm and HPU in mWm^{-3}.

Oxides	MR/1	MR/2	MR/3	MR/4	MR/5	MR/6	MR/7	MR/8	Crust2	Granite1
SiO_2	71.9	71.05	71.26	71.43	69.9	71.74	70.81	67.39	64.2	72.08
TiO_2	0.12	0.26	0.21	0.36	0.43	0.22	0.23	0.29	0.8	0.37
Al_2O_3	14.32	14.1	13.6	13.46	14.03	13.66	13.94	13.57	14.1	13.86
$FeO^{(T)}$	1.93	2.82	2.2	3.11	3.81	2.36	2.43	2.62	6.8	2.44
MgO	0.12	0.22	0.18	0.3	0.36	0.2	0.21	0.19	3.5	0.52
MnO	0.03	0.04	0.03	0.05	0.05	0.04	0.04	0.19	0.12	0.06
CaO	1.38	1.42	1.19	1.39	1.6	1.28	1.26	0.04	4.9	1.33
Na_2O	1.53	1.29	1.35	0.89	0.92	1.3	1.14	1.15	3.1	3.08
K_2O	6.35	6.36	6.25	6.87	6.96	6.1	6.02	6.94	2.3	5.46
P_2O_5	0.01	0.01	0.01	0.01	0.01	0.01	0.01	0.01	0.18	0.18
Total	97.69	97.57	96.28	97.87	98.07	96.91	96.09	92.39	100.00	99.38
Calculated Numbers										
A/CNK	1.2	1.22	1.22	1.24	1.17	1.25	1.31	1.25		
A/NK	1.53	1.57	1.54	1.61	1.55	1.59	1.66	1.55		
AI.	0.66	0.64	0.66	0.66	0.64	0.64	0.60	0.64	0.54	0.79
K/Rb	250.98	214.59	199.52	162.68	191.92	187.52	192.92	193.30	276.70	302.16
Mg/(Mg+Fe)	0.93	0.91	0.90	0.89	0.89	0.90	0.90	0.91	0.29	0.14
B	37.67	55.10	42.99	60.81	74.49	46.11	47.48	51.22		
Solidification Index	12.33	11.94	10.83	11.34	12.04	11.59	11.61	10.03	28.65	10.80
LI	26.97	26.38	26.51	25.38	25.29	26.25	25.72	25.44	25.20	25.20
DI	77.68	76.31	85.74	75.44	81.54	85.64	84.77	84.27		
FI	85.84	84.34	86.46	83.93	83.12	86.05	85.04	86.99	86.52	86.52
HPU	22.78	14.90	14.31	2.38	5.25	13.25	11.36	2.99	1.00	2.89
Trace elements in ppm										
Sc	6	6	6	6	6	6	5	6	19	5
V	18	21	6	17	25	17	11	6	128	20
Cr	32	32	24	27	28	24	25	15	92	4
Co	2.75	9	5	14	15	8	7	23	24	1
Ni	43	27	24	19	27	19	23	7	46	0.5
Cu	28	27	22	29	23	19	25	23	38	10
Zn	32	37	15	20	41	21	32	14	81	1.5
Ge	7	6	6	6	5	6	6	26	1.5	1.3
As	14	10	11	5	6	8	10	6	3.1	1.5
Rb	210	246	260	325	301	270	259	8	69	150
Sr	94	103	89	94	110	97	93	298	285	285
Y	46	41	44	32	32	39	41	77	17.5	40
Zr	104	116	117	170	247	115	126	43	175	180
Nb	17	15	15	15	16	12	18	145	11	20

Table 3 continued

Oxides	MR/1	MR/2	MR/3	MR/4	MR/5	MR/6	MR/7	MR/8	Crust2	Granite1
Sn	3	8	5	8	3	9	6	3	1.5	1.5
Ba	194	377	236	658	615	413	344	22	614	600
Ce	91	3	14	3	3	24	17	3	60	100
Pb	93	83	89	69	56	85	74	358	15	20
Th	30	37	25	16	22	25	28	64	7.1	17
U	77	45	46	2.75	12	42	34	16	1.2	4.8
Th/U	0.39	0.82	0.54	5.82	1.83	0.60	0.82	4.00	5.92	3.54
Rb/Sr	2.23	2.39	2.92	3.46	2.74	2.78	2.78	3.87	0.24	0.53
Rb/Zr	2.02	2.12	2.22	1.91	1.22	2.35	2.06	2.06	0.39	0.83
Rb/Ba	1.08	0.65	1.10	0.49	0.49	0.65	0.75	0.83	0.11	0.25
R1	2706.35	2705.58	2741.60	2743.58	2589.79	2821.86	2833.32	2522.68		
R2	434.50	439.43	403.02	427.63	464.26	414.82	418.67	398.65		
CIPW Normative mineralogy										
Q	35.26	35.48	36.41	36.22	33.57	37.50	37.83	33.41	28.35	30.84
C	2.43	2.52	2.46	2.05	2.09	2.60	3.27	2.75		0.90
Or	37.53	37.59	36.94	40.60	41.13	36.05	35.58	41.01	13.59	32.27
Ab	12.95	10.92	11.42	7.53	7.78	11.00	9.65	6.35	26.23	26.06
An	6.81	7.01	5.87	6.86	7.90	6.31	6.21	5.67	17.76	5.42
Di									0.65	
Hy	1.07	1.50	1.17	1.66	2.01	1.30	1.34	1.30		0.15
Mt	1.40	2.04	1.59	2.25	2.76	1.71	1.76	1.90	9.11	0.62
Il	0.23	0.49	0.40	0.68	0.82	0.42	0.44	0.55	1.52	0.70
Wollastonite (Wo)									1.90	
Hematite (Hm)									0.52	2.01
Hypersthene en	0.07	0.10	0.07	0.12	0.12	0.10	0.10	0.10		0.15
Hypersthene fs	1.00	1.40	1.10	1.53	1.88	1.20	1.24	1.20		

Note: [1]Granite composition [28], [2]Bulk Continental Crust composition [29].

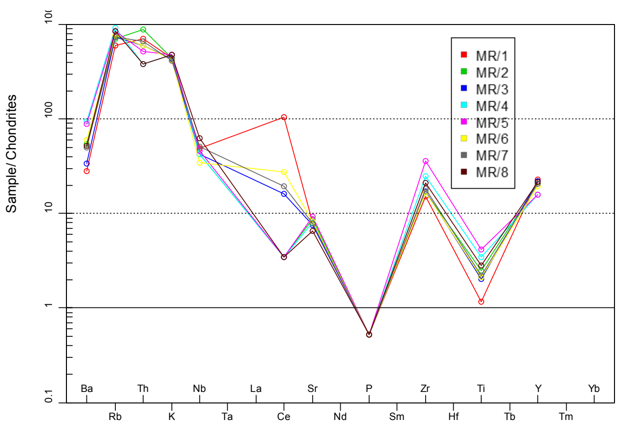

Figure 4a. Trace-element spider diagram for Mirgarani Granite Chondrite normalized after Thompson [30].

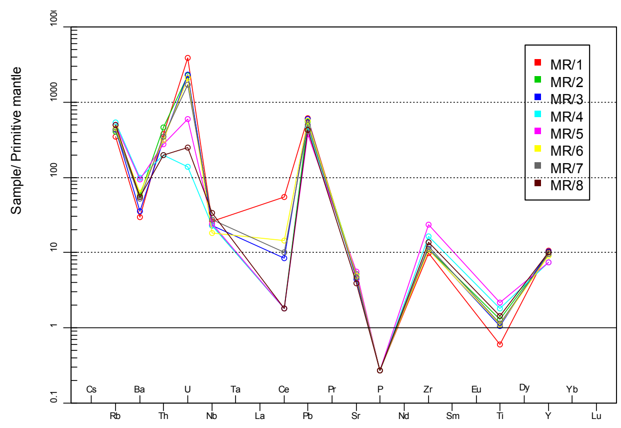

Figure 4b. Extended trace-element spider diagram for Mirgarani Granite Upper Crust normalized after MacDonough and Sun [31].

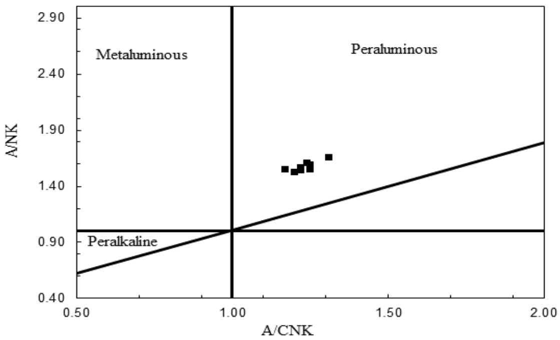

Figure 5a. A/CNK vs A/NK for Mirgarani Granite showing peraluminous character in Shands Index diagram modified after Maniar and Piccoli [32].

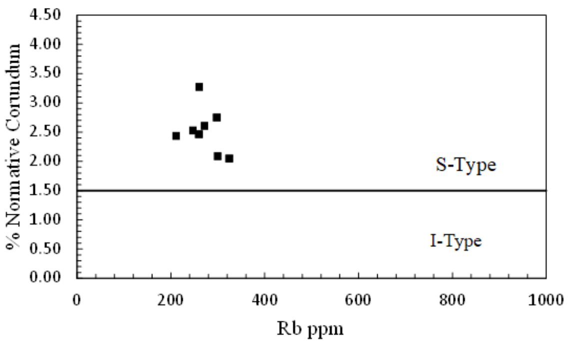

Figure 5b. Rb Vs Normative Corundum Plot for Mirgarani granite occupying S-type field.

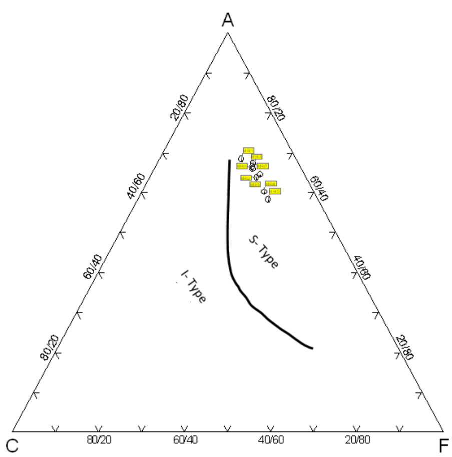

Figure 5c. ACF diagram showing S Type characteristics of Mirgarani Granite.

6. Petrogenesis

Mirgarani Granite is a Calc-Alkali to Alkali-Calcic granite with (Na_2O + K_2O)-CaO values varying from 5.9-6.54 with an average of 6.29. The total alkali (Na_2O + K_2O) versus SiO_2 TAS diagram (**Figure 6**) [33] shows that the Mirgarani granite is a subalkalic granite. The Na_2O + K_2O + Fe_2O_3 + MgO + TiO_2 vs. (Na_2O + K_2O)/(Fe_2O_3 + MgO + TiO_2) plot (**Figures 7a, 7b**) [34] shows evidence of a melt of crustal metagraywackes magma source. The experiments indicate that the meta-graywackes contain biotite and plagioclase but no aluminosilicates. The physical conditions of formation correspond to magmas formed by hybridization in the continental crust of normal thickness at depths of 30 km or less (**Figures 7a, 7b**) [34]. The plotting of MG on the Rb-Sr crustal thickness grid [35] suggests that the crust was thicker than 30 km during the evolution of Mirgarani granite (**Figure 8**).

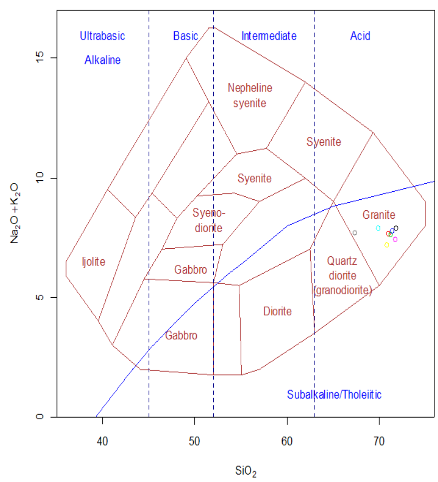

Figure 6. SiO_2 Vs Total Alkalies ($Na_2O = K_2O$) of Cox et al. [33] adopted by Wilson [36] for plutonic rocks. The curved line divides Alkalic and subalkalic rocks. The Mirgarani granite plots in a subalkalic Granite field.

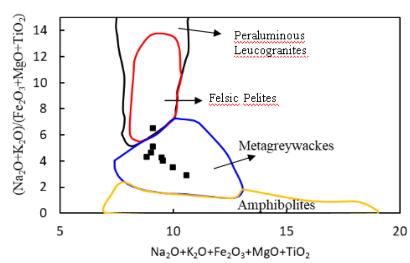

Figure 7a. The binary diagram Na_2O + K_2O + Fe_2O_3 + MgO + TiO_2 vs (Na_2O + K_2O)/ (Fe_2O_3 + MgO + TiO_2) after Patiño Douce [34]. Outlined are domains occupied by experimental granitic melts obtained by partial melting of metapelites, metagreywackes, and amphibolites (experiments of Patiño Douce [34] as summarized by Jung et al. [37]).

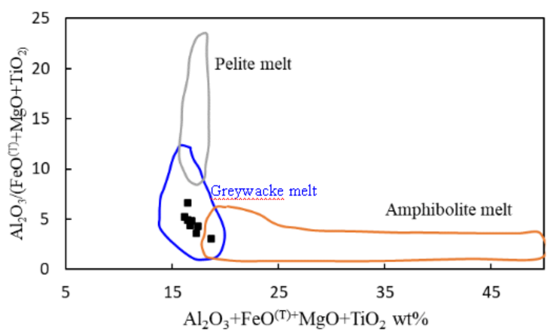

Figure 7b. Binary plot of $Al_2O_3 + FeO^t + MgO + TiO_2$ versus $Al_2O_3/(FeO^t + MgO + TiO_2)$. Outlined are domains occupied by experimental granitic melts obtained by partial melting of metapelites, metagreywackes, and amphibolite (experiments of Patiño Douce [34] as summarized by Jung et al. [37]).

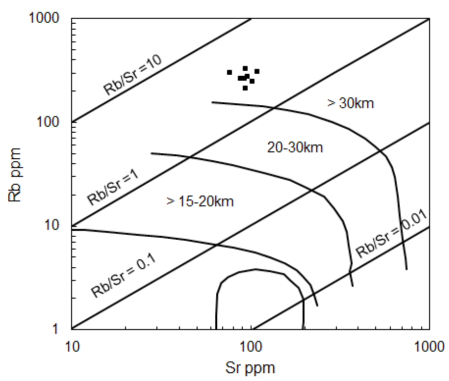

Figure 8. Plot of Rb Vs Sr for Mirgarani Granite the thickness grids after Condie 1973 [35].

A thicker crust increases the probability of crustal anatexis or partial melting of crustal material for the origin of granitic melts. This was further supported by the high initial $^{87}Sr/^{86}Sr$ ratio of 0.715 ± 0.012 (MSWD = 0.11). The presence of garnet and corundum in peraluminous S-type granites also indicates their derivation from the partial melting of sedimentary rocks that had experienced variable surface weathering [38-42]. A high Rb/Sr ratio of 2.23-3.87 with a mean of 2.9 indicates a peraluminous magma source [43]. The Rb-Ba-Sr diagram (**Figure 9**) [44] reveals that the MG is a normal to strongly differentiated granite, which is further supported by the modal plot of the Q-A-P diagram **Figure 3** [45]. The granite melts that created the Mirgarani granite were mainly moderately evolved to strongly evolved. K/Rb ratios of Mirgarani granite vary from 175.47-251.01 ppm with a mean of 200.80 ppm conforming to the K/Rb ratio (150-300) of the normal granite [46]. If the K/Rb ratio is under 100, the granite is highly evolved [47]. This observation occurs because Rb tends to be differentiated in the melt during the segregation stage of aqueous liquid phases from the remaining silicate melts [48]. The importance of K-feldspar, biotite, and plagioclase in differentiation is consistent with Large Ion Litho-modeling (LIL). LIL inter-element variation plots for Sr, Ba-Sr, and Ba-Rb pairs are shown in **Figures 10a and 10b**. Each plot also shows a vector plot representing the net change in the composition of the fluid after 30% Rayleigh fractionation due to the removal of K-feldspar, hornblende, plagioclase, or biotite. In all plots, the trend is consistent with the fractionation of plagioclase, K-feldspar, and biotite. Thus, the log-log plot of LIL suggests that crystal fractionation plays an important role in the magma evolution of the Mirgarani granite.

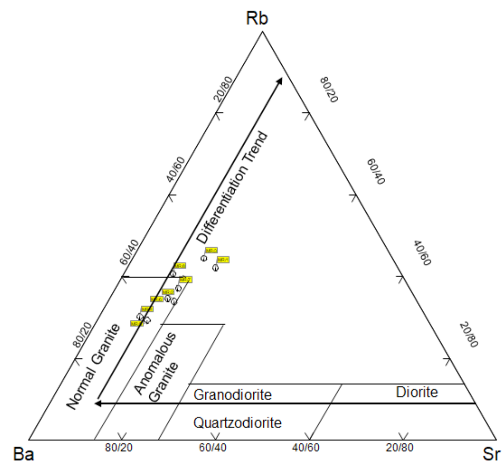

Figure 9. Rb-Ba-Sr Ternary diagram after El Bouseily and El Sokkary [44] reveals that the Mirgarani Granite falls in normal to strongly differentiated granite fields.

The most likely mechanism is crystal fractionation suggested by modeling (**Figures 10a and 10b**). The geochemical characteristics of some elements can be used to trace the materials of magmatic source regions. The Rb/Ba versus Rb/Sr discriminant diagrams (**Figure 11**) exhibit similar source material compositions—mainly clay-rich rocks (sandstone and shale) [51]. Pb-Ba data are plotted in **Figures 12a and 12b**, showing the samples fall in primary Low T, S-type also indicates the behavior of Pb during fractional crystallization.

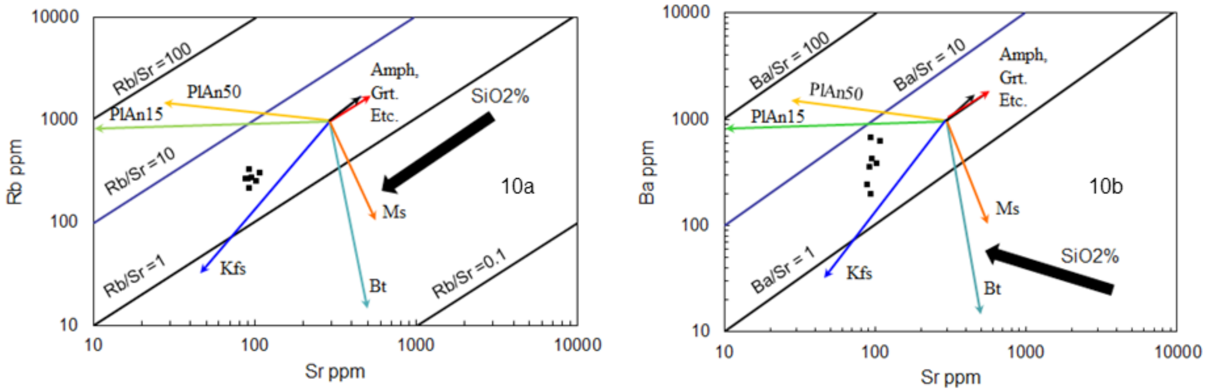

Figure 10. a: Plot of Sr vs. Rb, and **Figure 10b:** Plot of Sr vs. Ba after Rollinson,1993 [76], Janoušek et al., 2004 [83], An Anorthite, PL Plagioclase, Kf K-feldspar, Amph Amphibole, Grt Garnet, Bt Biotite, Ms Muscovite.The black arrow indicates the %SiO_2 variation.

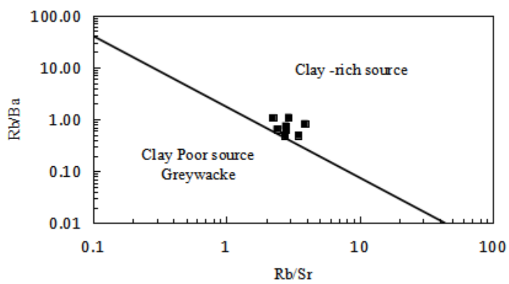

Figure 11. Rb/Sr vs Rb/Ba plot for Mirgarani granite showing its derivation from Clay rich source.

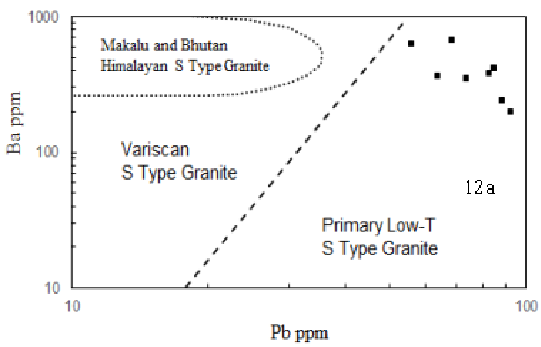

Figure 12a. Logarithmic Pb versus Ba diagrams for Mirgarani Granite showing data for the Makalu, Bhutan, Himalayan, Variscan, S-type granites [52,53].

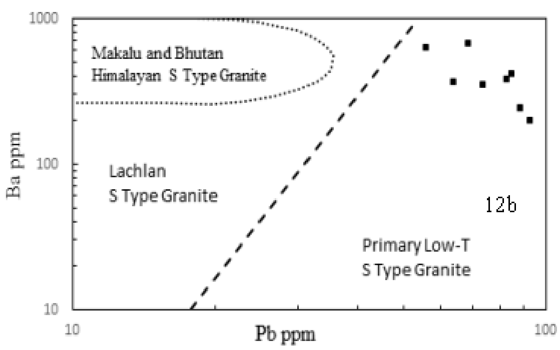

Figure 12b. Logarithmic Pb versus Ba diagram, and Lachlan S-Type granites and primary Low Ti S-Type granite.

7. Zircon saturation and temperature

Zircon behavior in magnetic systems has provided an understanding of magmatic processes and robust Petro-chronology. Watson and Harrison's [42,55] model was used to understanding the Zr saturation with respect to the cationic ratio M (M= Na + K + 2Ca/Al. Si) varies from 1.1 to 1.3 with an average of 1.2, Si, and Zr saturation temperature (**Figures 13a-13f**) clearly shows the fractionation trends. The zircon saturation temperature varies from 764 to 836 °C, with an average of 789 °C (**Table 4**). In the Ab-Or-Q granite system plot [56], the Mirgarani Granite samples occupy a temperature range of 685-700 °C, and M_2 represents the low-pressure granitic minimum at H_2O = 1000 bar [57] in **Figure 14**.

Table 4. Zircon saturation temperature of Mirgarani granite.

S. No.	M	Zr	Zr.sat	TZr.sat.C
MR/1	1.192221	104	87.6	764.1
MR/2	1.186905	116	87.2	773.7
MR/3	1.166125	117	85.7	775.9
MR/4	1.218428	170	89.6	804.8
MR/5	1.252666	247	92.2	836.7
MR/6	1.150865	115	84.6	775.6
MR/7	1.092356	126	80.5	787.7
MR/8	1.155939	145	85.0	795.3

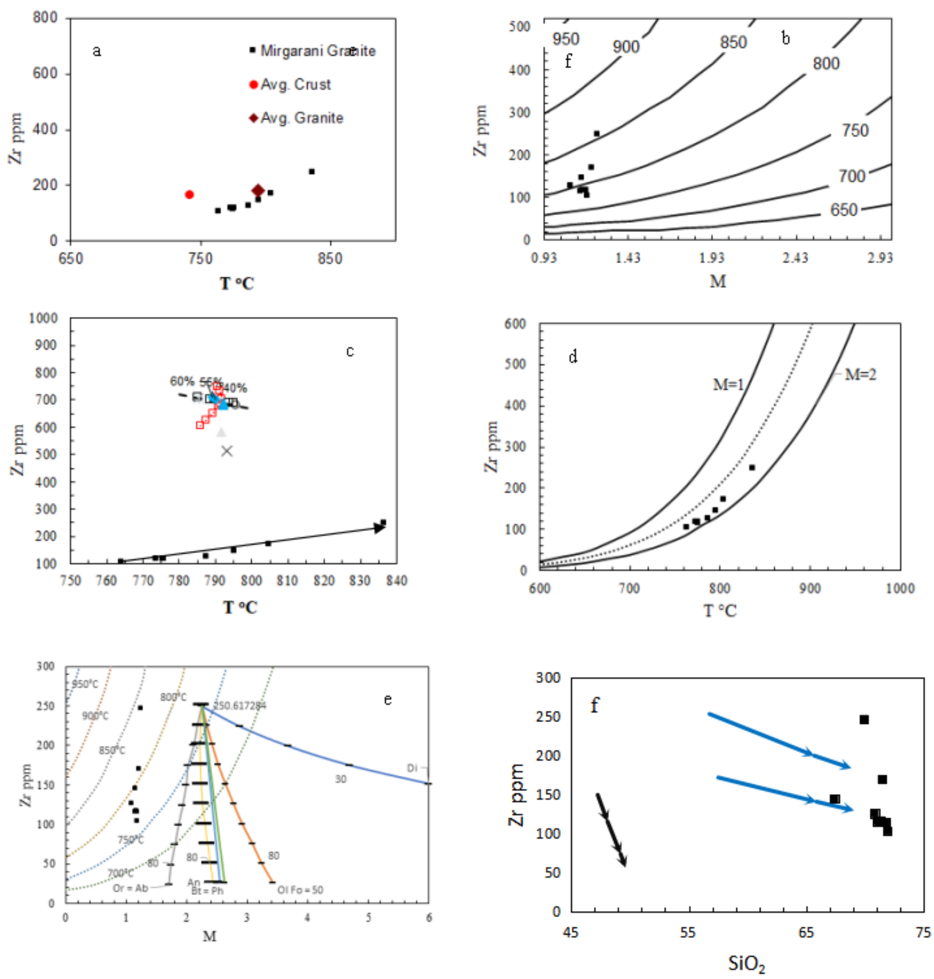

Figure 13. Temperature of crystallization of Mirgarani granite a: Temperature (TC) Vs Zr diagram, b: Binary plot of M=100 (Na+K+-2Ca)/Al*Si versus Zr saturation levels, c: Temperature Vs Zr showing fractionation trends, d: Temperature Vs Zr plots showing various M fields. e: M vs Zr, f: SiO_2 vs Zr with fractionation trends [54,55].

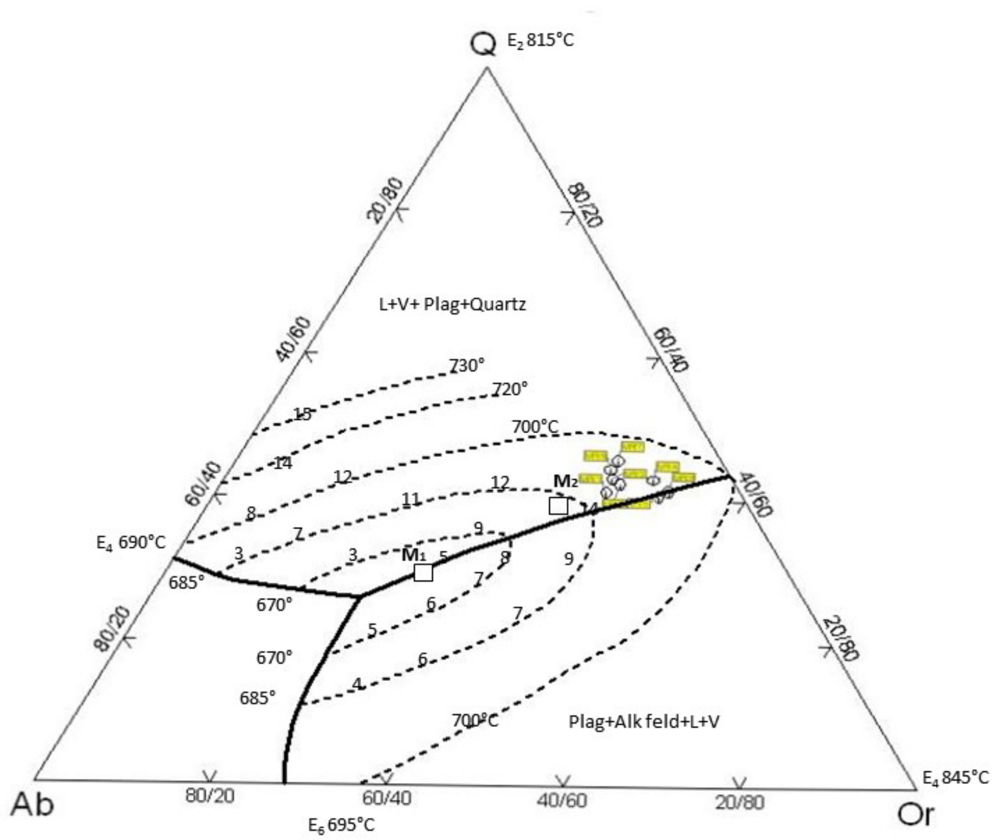

Figure 14. Quartz-Albite-Orthoclase ternary diagram of Mirgarani Granite after Winkler [56], M_1 minimum melt composition at pH_2O = 200bars, M_2 minimum melt composition at pH_2O = 100 bars at 5% An [57]. The numbers correspond to the ternary eutectic at 0.5 and 10 kb pressure, the lines joining eutectic compositions from the cotectic lines in the system. The numbers 3, 6, 9, 11 etc. denote the normative An contents.

8. Radiogenic heat production

Mirgarani granites show elevated levels of heat-producing elements (Th, U, K) and therefore have a high heat-producing capacity of 2.38 to 22.78 $mW \cdot m^{-3}$ with an average of 10.90 $mW \cdot m^{-3}$ (**Table 3**). The radiogenic heat production is calculated by the equation given by Wollenberg and Smith [58]. The unweighted mean of heat-producing capacity for the K-rich Arunta granites is about 6.5 $mW \cdot m^{-3}$ and the granites in the Paleozoic Lachlan Fold belt 3.1 $mW \cdot m^{-3}$ [41]. The bulk heat production in granitic rocks of all ages is ca. 2.0 $\mu W/m^3$. The Archean-Early Proterozoic granitic rocks 1.67 ± 1.49 and 1.25 ± 0.83 $\mu W/m^3$, respectively, and Middle Proterozoic granites presently 4.36 ± 2.17 $\mu W/m^3$, and Cenozoic granites 3.09 ± 1.62 $\mu W/m^3$ [59]. The comparison clearly shows that the Mirgarani granite has a higher heat-producing capacity than granite rocks of all ages, including early and middle Proterozoic granitic rocks, Arunta, and Lachlan fold belt granite. Because there is no specific boundary for defining HHP-type granites, the term HHP, as used here, has a comparative meaning (**Figure 15a**). For comparison, the average value of 6.5 $mW \cdot m^{-3}$ was arbitrarily set as the boundary for discrimination between the Main and HHP groups. **Figure 15b** shows the heat production capacity with respect to the SiO_2 wt.% for meta-sedimentary rocks. There is a decrease in heat production with SiO_2 for all metamorphic conditions for igneous rocks, but the differences within grades for rocks of similar SiO_2 do not show any consistent pattern. The curves for igneous and sedimentary rocks are shown in **Figure 15b**. A comparison of the HPU is shown in **Figure 15c**.

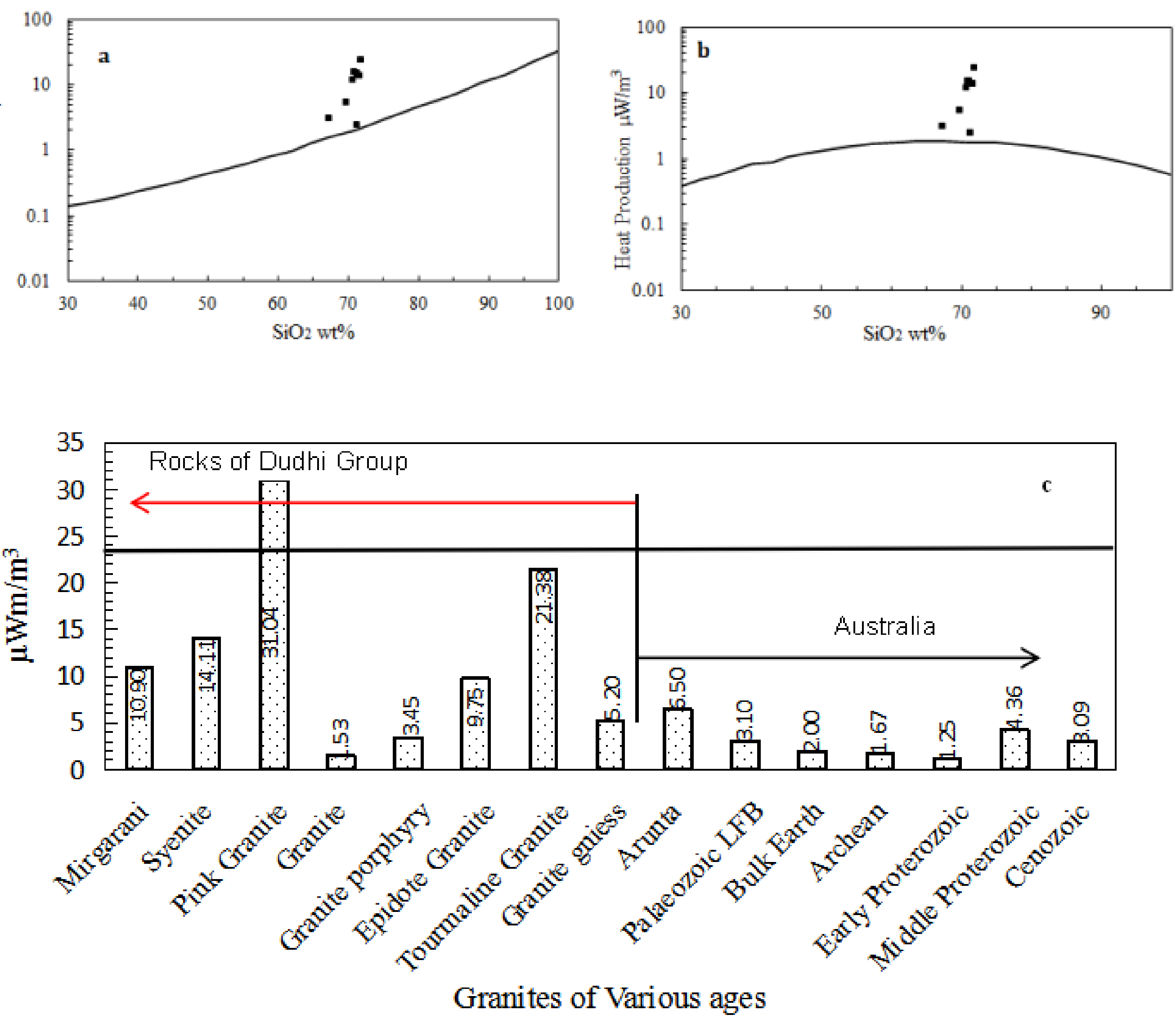

Figure 15. Heat production as a function of SiO_2 wt% with a heat production capacity of Mirgarani granite content. The curves are quadratic fit to heat production of igneous. **15a:** meta-igneous rocks and **15b:** metasedimentary rock samples as a function of metamorphic grade. Black curves are quadratic. For igneous rocks, the fit is constrained to 40 £ SiO_2 wt% £80 SiO_2 wt%; and for sedimentary rocks, the fit is constrained to £30 SiO_2 wt% £ 100 SiO_2 wt%. **15c:** Comparative bar chart of HPU of Granites of Dudhi Group with Australian Granites, Bulk earth, and granites of various ages.

9. Tectonic discrimination

Discriminant diagrams were used to ascertain the geotectonic environment in which the MG was emplaced. The Y + Nb vs. Rb plot (**Figure 16a**) [60]. The MG occupies within plate field (n = 6) with minor overlap in the syn collision granite (n = 2) field, whereas the Y vs Nb plot (**Figure 16b**) [60] occupies WPG (n = 5) to SCG + VAG (n = 3). In the R2 vs. R1 plots, the Mirgarani granite mostly falls in syn-collisional fields (**Figure 16c**). Therefore, the Mirgarani granite can be classified as within plate granite and can be correlated to the bimodal magmatism (Anorthosite-Granite) event in the CGGC during the late Paleo-Proterozoic to early Meso-Proterozoic i.e., ~ 1600 Ma [61].

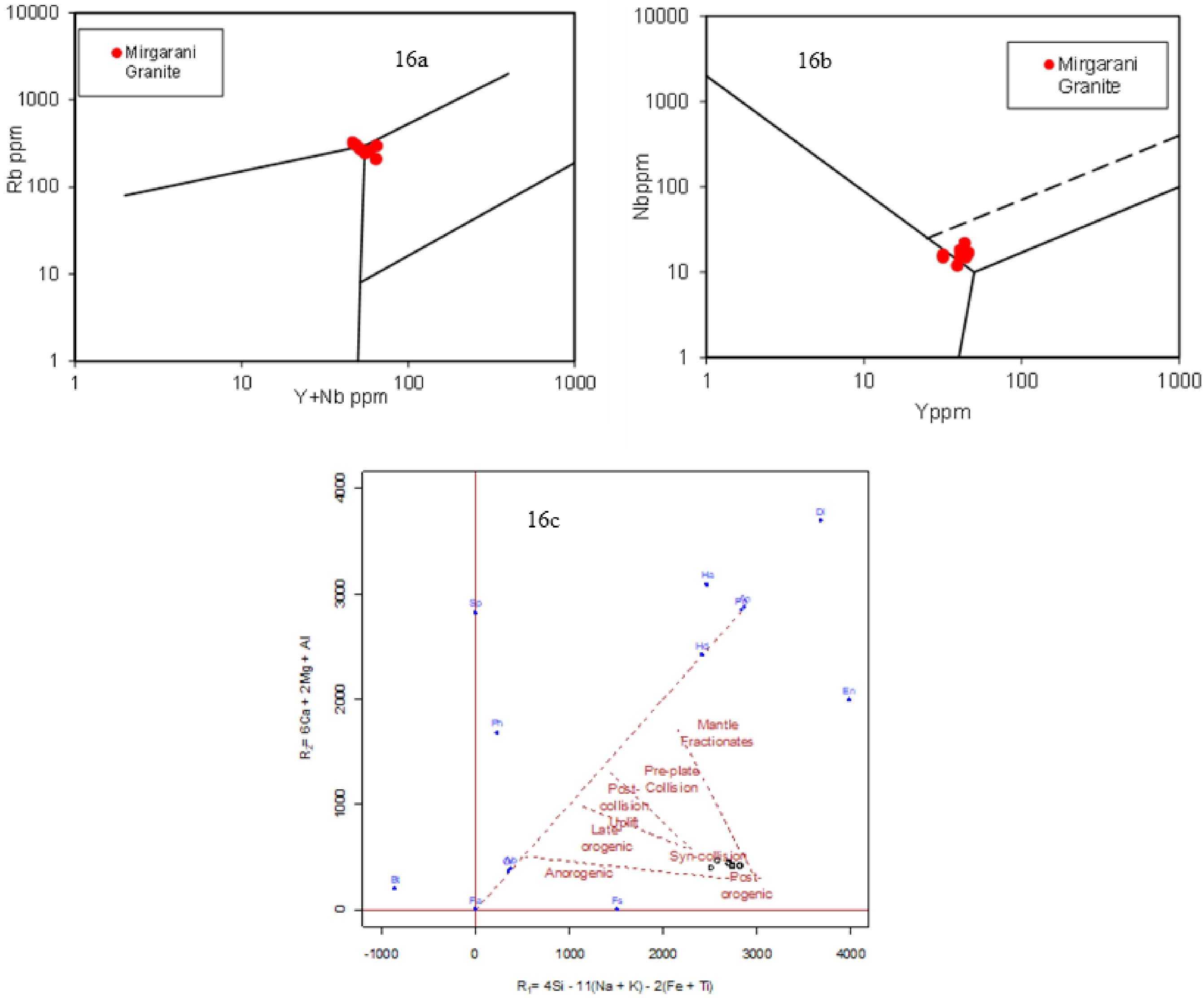

Figure 16. Tectonic discrimination plots for Mirgarani Granite, **16a:** Y+Nb Vs Rb plot showing CCG character, and **16b:** Y vs Nb Plot showing Syn collisional Granite field fileds [60]. **16c:** R_1-R_2 Plot showing syn-collisional origin for Mirgarani Granite Such rocks were generated by partial melting of the deep crustal rocks and intruding in the early stages of major intracontinental rifting during the mid-Proterozoic [62] or into the thickened overriding plate of a continental collision mobile belt [63].

10. Geochronology

The eight samples of Mirgarani granite were collected from Mirgarani hillock and analyzed for Rb-Sr isotopes on thermal ionization source, multi-collector computer-controlled VG-354 mass spectrometer. The standard exchange technique was followed for the separation of Rb and Sr from the powdered rock samples. Rubidium and Strontium contents of the samples (**Table 6**) were measured by conventional isotopic dilution technique as discussed by Gupta et al. [64]. $^{87}Rb/^{86}Sr$ of eight samples has been plotted against the Sr ratio (**Figure 17a**). The straight line obtained defines the isochron age of 1636 ± 66 Ma with an initial Sr ratio of 0.712 ± 0.012 with MSWD 0.11. Strontium evolution in CGGC has been attempted by integrating all the Rb-Sr isotopic data available in CGGC, particularly in the northwestern and western parts of the CGGC. The relevant data are conveniently displayed on the $^{87}Sr/^{86}Sr$ development diagram (**Figure 17b**). The simplest model for crustal formation involves continuous mantle-to-crust evolution on the one hand and two-stage evolution on the other. Isotopic research should permit the assessment of these models; no clear picture has so far emerged, perhaps because of the recycling of crustal material through the mantle [65]. A development line is defined by a regular trend of initial $^{87}Sr/^{86}Sr$ ratios, as a function of time, from a family of related rock systems. The two-stage model advocates the formation of most of the sialic crust from the upper mantle early in the Earth's history, with younger granitic rocks forming largely by anatexis of this primitive crust [66,67]. The development line for the upper mantle has been represented by [68] line AB in **Figure 17b**. In contrast, if formed in one episode early in the Earth's history, the development line for the entire sialic crust would be represented by a line of much steeper slopes. Using the estimated average Rb/Sr ratio for the sialic crust of 0.15 [65], this line is represented by C'D' in **Figure 17b**. The alternative simple model advocates the continued formation of new continental sialic crust in many episodes of differentiation from the upper mantle, with only minor amounts being formed by anatexis of older continental rocks [69,70]. The development line for the mantle beneath a large volume of such sialic crust may be represented by a curve or succession of straight lines, initially of steep attitude but following a successively gentler slope with time. On this hypothesis a steep vector for crustal rocks would represent only one of the many granite-forming events; it would be restricted to a small volume of crust that originated in a single upper mantle differentiation event. A recent exposition of this hypothesis [71] invoked an environment of plate convergence and a sequence of subduction, partial melting of the mafic lithosphere, and extraction of basaltic and calc-alkalic rocks, with resulting accretion of new continental crust. Repeated reworking of significantly older sialic crust—with anything like normal Rb/Sr ratios—is rejected; the basic hypothesis precludes the possibility of large volumes of different lower Precambrian granites, whose individual ages range over a substantial time interval (say, 500 m.y.), yielding initial $^{87}Sr/^{86}Sr$ ratios on a straight line of a steeper slope than the upper mantle development line. Both models postulate the beginning of the formation of extensive continental sialic crust in the period from 3,000 to 3,500 m.y. ago. Since these models were formulated, Rb-Sr and U-Pb age determinations from several areas have extended the upper limit back to sometime around or before 3,700 m.y. ago.

Table 6. Rb-Sr data on Mirgarani granite.

Sample No.	**Rb ppm**	**Sr ppm**	**87Rb/86Sr**	**87Sr/86Sr**
MR1	257	55.3	13.9	1.04237
MR2	258	58.2	13.26	1.02732
MR3	253	53.5	14.18	1.04942
MR4	258	56.9	13.54	1.035206
MR5	246	72.6	10.04	0.94999
MR6	259	76.8	9.998	0.94964
MR7	264	51	15.54	1.08066
MR8	253	47.2	16.1	1.08823

Error: 1% in Rb and Sr values, 2% in $^{87}Rb/^{86}Sr$, and 0.05%in $^{87}Sr/^{86}Sr$.

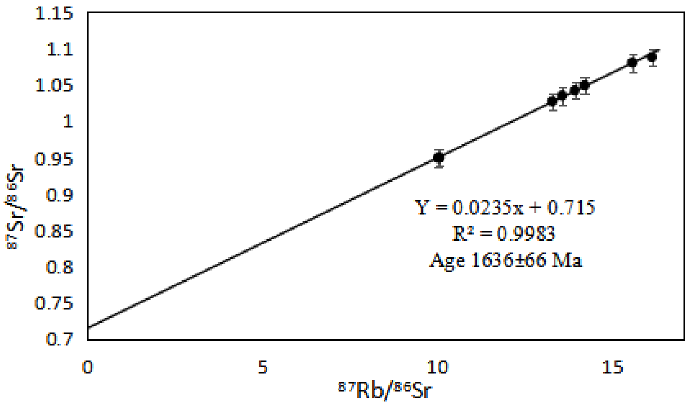

Figure 17a. Rb-Sr Isochron plot for Mirgarani granite.

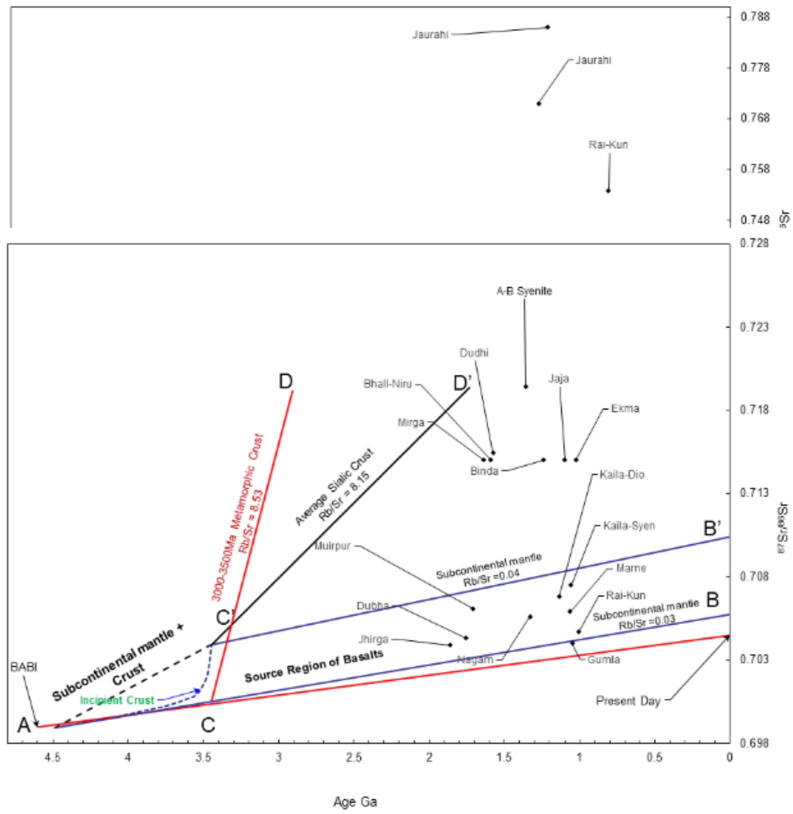

Figure 17b. Diagram showing the variation of the initial $^{87}Sr/^{86}Sr$ ratio with age. Vectors from each point, length immaterial, indicate the direction of isotopic evolution with time; calculated from the mean Rb/Sr ratios for each suite. Suboceanic and subcontinental mantle development lines shown were proposed by Davies et al. [70]; they are bounded by achondrite value (A), the mean value for recent oceanic tholeiites (B), and extension of the trend of values for mafic rocks in southern Africa (B'). It is proposed that the "source region of basalts" field is bounded *by* these two development lines. Hypothetical development line C'D' for average sialic crust conforms with a two-stage model involving a major mantle-crust differentiation about 3500 m.y. ago; this line intersects T = 0 axis at $^{87}Sr/^{86}Sr = 0.725$. The Red line shows $^{87}Sr/^{86}Sr$ ratio (0.69897 ± 0.00003) evolution from BABI to the present day The other parameter for UR model is $^{87}Rb/^{86}Sr$ ratio of the bulk earth is 0.0816 and the present-day Sr value is 0.7045.

11. Discussions

Petrochemical characteristics, field setting, and cogenetic granites and granitoids of Dudhi Group which form the northwestern part of CGGC, and a review of the geochronological data (**Table 7**) show five phases of granitic activities. The first phase of granitic activity dates from the Gaya area, the age of the Satpura orogenic cycle was considered to be 955 Ma [72,73]. The Chhotanagpur plateau has been formed due to the three successive phases of orogeny during the middle to late Proterozoic time. These orogenic movements have deformed the area in three successive phases.

The CGGC is dissected by three major lineaments (**Figure 18a**). The South Purulia Shear Zone (SPSZ) and Monghyr-Saharsa Ridge Fault roughly coincide with the southern and northwestern boundaries of the CGGC respectively. The lineament, that bound the exposure of Gondwana deposits of Damodar valley runs through Domain I of the CGGC [74] and is hereafter termed Gondwana Boundary Faults (GBF) (**Figure 18a**). Using the GBF as a marker, Domain I is further divided into two geographic sub-domains viz. Domain IA (south) and IB (north) by GBF and southern boundary fault of Gondwana Graben and Jajawal Shear zone. Accessibility issues led to a dearth of geochronological data from the western and northwestern regions of CGGC. The Son-Narmada South Fault (SNSF) and North Fault (SNNF) cause radiometric breaks in the radio-geochemical images based on airborne gamma-ray spectrometric data in the Son-Valley area, where the Mahakoshal group of volcano-sedimentary rock have deposited in the rift valley known as Son Valley. These faults have NE-SW, East-West, and ENE-WSW trending faults [20]. Mirgarani granite is coeval to the granites in Bihar Mica Belt (BMB) around the Bhallupahari-Nerupahar, Hazaribagh area dated 1590 ± 30 Ma [75]. High-precision U-Pb SHRIMP zircon $^{206}Pb/^{238}U$ ages for Microgranular Enclave (1758 ± 19 Ma) and host granitoid (1753 ± 9.1 Ma) from Jhirgadandi Pluton further support that they were coeval. Jhirgadandi granodiorite (Jh) is dated by Rb-Sr whole-rock method 1860 ± 180 Ma with an initial Sr ratio of 0.7039 ± 38 [76]. Other coeval granitoids in the area are Jhirgadandi granitoid (Jh; 1753-1880 Ma), Tumiya granitoid (T; 1780 Ma), and Neruiyadamar granitoid (N; ca. 1880 Ma) within the Mahakoshal group whereas, Harnakachar granitoid (H; 1710 Ma), Katoli granitoid (Ka; 1730 Ma), ± 9.1 Ma, Dudhi Granite; 1750 Ma, Raspahari granitoid (R; ca. 1750 Ma) are in the Dudhi Group. Ainti-Bari syenites dated by Rb-Sr method as 1360 ± 30 Ma with $^{87}Sr/^{86}Sr$ ratio of 0.7194 ± 12 [75]. High Rb and Low Sr Riebeckite granites at the Jaurahi area gave an isochron age of 1280 ± 78 Ma with $^{87}Sr/^{86}Sr$ ratio 0.771 ± 0.039 with MSWD 21. However, the Low Rb and High Sr Riebeckite granites of all the samples considered together then gave an isochrone age of 1219 ± 74 Ma with $^{87}Sr/^{86}Sr$ ratio of 0.786 ± 0.048 with a very high MSWD 56. The Pb-Pb isotopic isochrone age was found at 1219 ± 190 Ma with model μ8.3 ± 0.2 and MSWD of 9.1. It is therefore taken as 1290 ± 190 Ma [77]. Makrohar granulite 1700-1580 Rb-Sr whole-rock isochron ages [78]. Kirwil-Sagobandh Mafic Granulites dated 1648 ± 112 Ma with $^{87}Sr/^{86}Sr$ ratio of 0.70202 ± 0.00032 with MSWD 0.040 [23]. Both of these granulites i.e. Makrohar and Kirwil Sagobandh show post peak isobaric cooling events in the area. Other Granulites in CGGC are in **Table 7**. The IBC pathways > 1457-1648 Ma while the ITD paths are < 1447-930 Ma [11,21,23,78,80,81].

Barambaba granite 1690 ± 70 Ma Rb-Sr age [82], Rihand granite 1731 ± 36 Ma and Vikasnagar granite and Kundabhati granites have Rb-Sr ages of 1717 Ma, and 900-1292 Ma, respectively [79], also the Purulia granites and syenites of Jamua-Dumka sector Bihar are dates 1331 ± 125 [80]. Muirpur Granite five sample whole-rock defines Rb-Sr isochron age of 1709 ± 102 Ma with an initial $^{87}Sr/^{86}Sr$ ratio of 0.70609 ± 342 and MSWD of 0.59 [78], Dudhi Granite Gneiss's six whole-rock samples define an Rb-Sr isochron age of 1576 ± 76 Ma with an initial $^{87}Sr/^{86}Sr$ ratio of 0.71543 ± 89 and MSWD of 0.29 [75]. The Mahakoshal Belt experienced a period of relaxation marked by vast post-collisional episodic magmatism 1880-1710 Ma and forming the Neruiyadamar Granitoid (1880 Ma) and Jhirgadandi granite (1860 Ma, 1753 ± 9.1 Ma), Dudhi Granite gneiss (1750 Ma), Raspahari granitoid (ca. 1750 Ma), Katoli granitoid (1730 Ma) and, Tumiya Granitoid (1780 Ma), Harnakachar granitoid plutons (1710 Ma) of the Mahakoshal Belt [83,84]. These Rb-Sr ages around 1636 to 1880 Ma can be correlated to the Chhotanagpur orogeny and Columbia-Nuna supercontinent.

Table 7. Age data on Chhotanagpur granite Gneiss complex.

Geological Time	Rock types and locality	Methods	Age (Ma)	Reference	LIPs
	Phase V				
Mesozoic (251-66 Ma)	Sylhet Traps	K-Ar	110 ± 3, 133 ± 4	Sarkar et al., 1996 [102]	
	Rajmahal Traps		117 ± 2	Bakshi, 1995 [95]	
	Lamprophyre dykes Minnet and Lamproite Jhariya and Raniganj Rajmahal.	$^{40}Ar/^{39}Ar$ dating	113 ± 7	Sarkar et al., 1980 [114]	
	Dykes intruded on the SW of the Rajmahal Hills	$^{40}Ar/^{39}Ar$ dating	115-118	Kent et al., 2002 [116]	
	Dolerite Dyke near Latehar railway station	K-Ar	185	Ghose et al., 1973 [98]	Wegner's Pangea c.325-175 Ma
	Phase IV				
	Rhyodacite, Mahuandanr-Rajdanda	K-Ar	217-214	Sarkar, 1974, [99]	
Paleozoic (541-251)	Enstatite/Hornblende Peridotite, Pyroxinite and Hornblendite, Richughuta (unmetamorphosed)	K-Ar	275	Ghose et al., 1973 [98]	
	Phase III				
	Aphanitic Quartz rich granite aplite	K-Ar	353	Ghose et al., 1973 [98]	Gondwanaland/ Pannotia (620-580 Ma) Cryogenian Period (ca. 720-635 Ma)
	Syenite, Nepheline syenite and Alkali granite.	K-Ar	435		
Neoproterozoic (1000-541 Ma)	Phase II				
	Allanite Puruliya Bihar Allanite Bahea Singar Bihar	U+Th-Pb	880 880	Nandi and Sen, 1950 [90]	
	Pegmatite, Dumhat	Rb-Sr whole-rock Isochron	886, 932, 941	Pandey et al., 1986a [86]	Rodinia (1100-700 Ma)
	Mica Granite	Rb-Sr Mineral Age	855 ± 25		
	Kunkuri, Raigarh Raikera-Kunkuri	Rb-Sr WR	803 ± 49, 815 ± 47, 1005 ± 51	Singh and Krishna, 2009 [97]	
	Leucogranite Muscovite, Belamu-Jaipur	K-Ar	810 ± 40	Baidya and Chakravarthy, 1988 [96]	
	Pegmatite Columbite -Tantalite, Dhajua pegmatite etc.	U-Pb, Pb-Pb Mineral	910 ± 19	Krishna et al., 2003, [83]	
	Singar Gaya Uraninite from pegmatite	U+Th-Pb	955 ± 40	Holmes et al., 1950 [89]	
Neoproterozoic (1000-541 Ma)	Pichali Bihar, Monazite Magnetite Chaibasa Bihar	U+Th-Pb Alpha-Helium	970 970	Nandi and Sen, 1950 [90] Krishnan et al., 1953 [92]	
	Raigarh Granite II (Kunkuri)	Rb-Sr WR	972 ± 114	Pandey et al., 1998 [79]	

Table 7 continued

Geological Time	Rock types and locality	Methods	Age (Ma)	Reference	LIPs
Neoproterozoic (1000-541 Ma)	Uraninite from Bihar Mica Belt	U+Th-Pb	960 ± 50	Vinogradov et al., 1964 [88]	
	Kundabhati Granite	Rb-Sr	900-1292	Pandey et al., 1998 [79]	
	Monazite from Gaya Allanite from Ranchi	U-Pb U-Pb	965 Ma 980 Ma	Sarkar, 1941 [91] Lal et al., 1976 [94]	
	Migmatitic Quartzo- Feldspathic Gneiss, NE Dumka Near N. margin of CGGC, ITD	Monazite in Garnet Matrix	984-930 Ma	Chatterjee et al., 2010 [12]	
	Basic Granulites, Bero N. Purulia, ITD, 11 to 5kbar	U-Pb Monazite	990-940 Ma	Karmakar et al., 2011 [81]	
Mesoproterozoic (1600-1000 Ma)	Phase I				
	Uraninite	U+Th/Pb	1000 Ma	Vinogradov et al., 1964 [88]	
	Purulia Granite	Rb-Sr WR	1071 ± 64	Ray Barman et al., 1994 [80]	
	Gumla granite	Rb-Sr WR	1051 ± 272, 1048 ±135	Pandey et al., 1998 [79]	
	Ekma Granite	Rb-Sr WR	1025 ± 11	Singh and Krishna, 2009 [99]	
	Alkali syenite, Kailashnathgufa	Rb-Sr WR age	1059 ± 104	Pandey et al., 1998 [79] Singh and Krishna, 2009 [97]	
	Marme pink granite	Rb-Sr WR	1065 ± 74	Singh and Krishna, 2009 [99]	
	Jajawal Granite Gneiss	Rb-Sr WR	1100 ± 20	Pandey et al., 1986b [87]	
	Chianki granite gneiss	Rb-Sr WR	1119 ± 24	Singh and Krishna, 2009 [97]	
	Raigarh diorite, Kailashnathgufa	Rb-Sr WR	1138 ± 193	Pandey et al., 1986b [87] Singh and Krishna, 2009 [97]	
	Migmatitic Gneisses, Jamua-Dumka, ITD	Rb-Sr WR	1178 ± 68 Ma	Ray Burman et al., 1994 [80]	
	Migmatitic Granite gneiss, Hesatu–Belbathan area	Rb-Sr whole-rock	1300-1110	Pandey et al., 1986 a, b [86,87]	
	Binda-Nagnaha, Granite-gneiss	Rb-Sr whole-rock	1242 ± 34	Pandey et al., 1986a [86]	Break up of Columbia/Nuna 1.5-1.2 Ga
Paleoproterozoic 2500-1600 Ma	Granite and Riebeckite Granites Granite and Riebeckite Granites	Rb-Sr WR Pb-Pb WR	1219 ± 74, 1280 ± 78 1219 ± 130	Sastry et al., 2017 [77]	
	Raigarh I Nagam granite	Rb-Sr, WR	1331 ± 42	Singh and Krishna, 2009 [97]	
	Syenite	Rb-Sr, WR	1331 ± 125	Ray Burman et al., 1994 [80]	
	Migmatitic granite gneiss, NE part of the CGGC	K-Ar whole-rock age dating;	1416-1246	Sarkar, 1980 [9]	
	Dumka granulite	Rb-Sr WR	1331 ± 125	Ray Burman et al., 1994 [80]	
	Charnockite Gneiss, Jamua-Dumka Sector Purulia, ITD	Rb-Sr WR	1447 ± 11 Ma		
	Charnockite Gneiss, Deoghar–Dumka, IBC	Rb-Sr WR	1457 ± 63 Ma	Ray Burman et al., 1994 [80] Mukherjee et al., 2019 [16]	Columbia / Nuna 1.9-1.6Ga
	Dumka syenite	Rb-Sr WR	1457 ± 63	Ray Burman et al., 1994 [80]	
	Mica belt granite I, Bhallupahari-Nirupahari	Rb-Sr WR	1590 ± 30	Pandey et al., 1986a [86]	

Table 7 continued

Geological Time	Rock types and locality	Methods	Age (Ma)	Reference	LIPs
Paleoproterozoic 2500-1600 Ma	Mor Valley migmatite	Rb-Sr WR	1580 ± 33	Sarkar et al., 1998 [78]	
	Massive charnockite Basic granulite- Jamua–Dumka, Purulia IBC	Rb-Sr whole-rock isochron	1515 ± 5, 1000 1515	Ray Burman et al., 1994 [80]	
	Dudhi Granite gneiss	Rb-Sr WR	1576 ± 76	Sarkar et al., 1998 [75]	
	Mor valley	Rb-Sr WR	1599-1522	Mallik et al., 1991 [85]	
Paleoproterozoic 2500-1600 Ma	Hypersthene Gneiss, IBC	Rb-Sr WR	1624 ± 5 Ma	Sarkar et al., 1998 [78]	
	Massive Charnockite and Basic Granulites, Jamua-Dumka Sector Purulia, IBC	Rb-Sr WR	1624 ± 5, 1000	Ray Barman et al., 1994 [80]	
	Barambaba granite	Rb-Sr WR	1690 ± 70	Jain et al., 1995 [82]	
	Mirgarani granite	Rb-Sr WR	1636 ± 66	Present Study	
	Kirwil-Sagobandh Mafic Granulites, Post-peak IBC path	Rb-Sr WR	1648 ± 112	Dhurandhar et al., 2003, 2006 [20,22]	
	Makrohar granulite, IBC, 7-7.5 kbar	Rb-Sr WR	1700-1580	Sarkar et al., 1998 [75]	
	Harnakachar granitoid	U-Pb SHRIMP	1710 Ma	Bora and Santosh, 2015 [84]	
	Vikasnagar Granite	Rb-Sr WR	1717 Ma	Pandey et al., 1998 [79]	
	Katoli granitoid	U-Pb SHRIMP	ca.1730 Ma	Bora and Santosh, 2015 [84]	
	Rihand granite	Rb-Sr WR	1731 ± 36	Sarkar et al., 1998 [78]	
	Muirpur granite	Rb-Sr WR	1709 ± 102		
	Raspahari Granitoid	U-Pb SHRIMP	ca. 1750 Ma	Bora and Santosh, 2015 [84]	
	Dubha granite	Rb=Sr WR	1754 ± 16	Dhurandhar et al., 2005 [22]	
	Metapelitic granulite. Southern margin of CGGC	Rb-Sr WR	1741 ± 65	Ray Barman et al., 1994 [80]	
	Tumiya Granitoid In Mahakoshal Group	U-Pb SHRIMP	ca.1780 Ma	Bora and Santosh, 2015 [84]	
Paleoproterozoic 2500-1600 Ma	Tatapani gray migmatite	Rb-Sr WR	1787 ± 72	Hansoti and Deshmukh, 1990 [24]	Columbia / Nuna 1.9-1.6Ga
	Jhirgadandi Granite-Granodiorite in Mahakoshal Group	Rb-Sr WR U-Pb SHRIMP	1860 ± 180 Ma 1753 ± 9.1 Ma	Pandey et al., 2004 [76] Bora et al., 2013 [83] Bora and Santosh, 2015 [84]	
	Neruiyadamar Granite in Mahakoshal Group	U-Pb SHRIMP	ca 1880 Ma	Bora and Santosh, 2015 [84]	

The radioactive minerals are dated around 800-900 Ma typically during Phase II i.e. Uraninite from Gaya Bihar 960 ± 50 [88], 955 ± 40 Ma from Singar [89], Pichali Monazite 970 [90], Gaya monazite dated 965 Ma [91], and Magnetite from Chaibasa also dated 970 Ma [92], Columbite and Tantalite in pegmatite are dated 910 ± 19 by U-Pb, Pb-Pb Mineral methods [93]. Allanite from Ranchi dated 980 Ma [94], and from Singar and Puruliya both are dated 880Ma by the U-Pb method [95]. Moreover, the Pegmatites from these areas viz. Belamu, Jaipur 810 ± 40 by K-Ar method [96], and Kunkuri Raigarh and Raikera area, also dated between 800 to 941 Ma by Rb-Sr isochron methods [97] but these have very high initial strontium ratio indicating a higher degree of crustal contamination (**Table 7** and **Figure 17b**). These episodes correlate well with Rodinia supercontinent.

Phase III is marked by the intrusion of alkaline magma such as Syenite, Nepheline Syenite, and alkali granites dated 435 Ma and Aphanitic Quartz rich granite aplite dated 353 Ma both by K-Ar methods [98].

Phase IV begins with the hornblende peridotite, pyroxenite hornblendite dated 275 Ma by K-Ar method [98] and Rhyodacite, Mahuandanr – Rajdanda area dated 214-217 Ma [99].

Finally, Phase V is marked by extrusives like dykes of Latehar 185 Ma, SW of Rajmahal 115-118 Ma, Lamprophyre and Minnet Lamprophyres Jhariya and Raniganj area dated by $^{40}Ar/^{39}Ar$ 113 ± 7 Ma [100], and volcanic of Rajmahal 117 ± 2 [101] and Sylhet Traps 110 ± 3 to 133 ± 4 Ma in northeastern India [102]. Phases III, IV, and V are related to Pan-African activities and the Pangea breakup.

12. Implications for super continental amalgamation and fragmentations

The evolution of earth's history shows that several supercontinents assembled and broken up viz. 3.0 Ga Ur [103] c. 2.7-2.5 Ga Kenorland; [104]; Lauroscandia; [105]. c. 1.9-1.75Ga Nuna or Columbia assembled or perhaps 1.6 Ga, and fragmented during the interval 1.3-1.2 Ga [106-108]. Rodinia supercontinent was being drafted, based on the growing recognition of correlatable mid-Neoproterozoic (0.8-0.7 Ga) rifted passive margins, many of which were established on the eroded remnants of late Mesoproterozoic (1.3-1.0 Ga) orogenic belts [109]. c. 950-800 Ma Rodinia [110], Rodinia Supercontinent existed from 1000 to 725 Ma. The Cryogenian Period ca. 720-635 Ma, which occurred about 700 Ma may have been a result of the breakup of Rodinia that began about 725 Ma [111], and the subsequent amalgamation of Gondwanaland. c. 620-580 Ma Gondwanaland/Pannotia [112,113]; the break out of Laurentia from Rodinia at 725 Ma marks the re-organization of lithospheric plate motion that resulted in the Pan-African-Brasiliano orogeny.

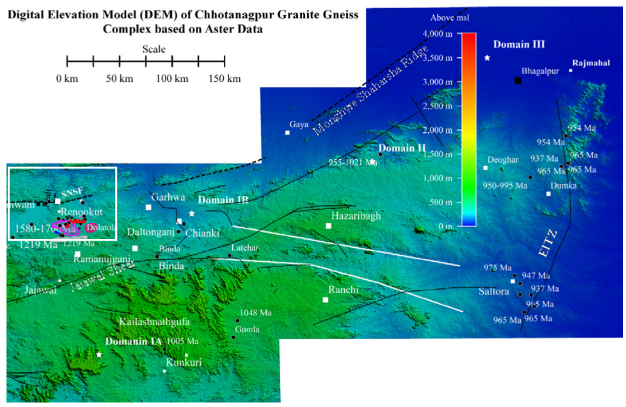

Figure 18a. Digital Elevation Model (DEM) of Chhotanagpur Granite Gneiss Complex showing major tectonic lineaments and study area.

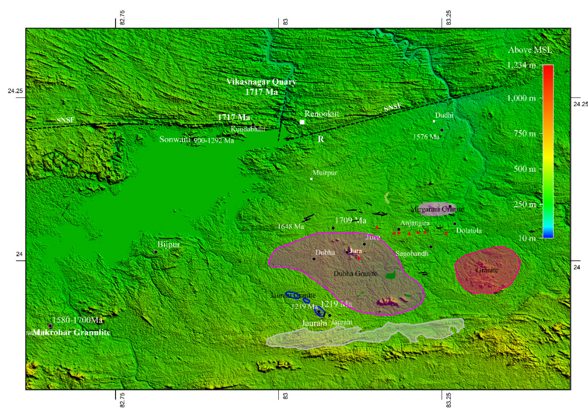

Figure 18b. DEM of Dudhi Group showing ages of various rock types, R: Raspahari Granitoid, Ka: Katoli Granitoid, H: Harnakachar Granitoid.

The formation of Gondwanaland and breakups are debated [114,115] as under:

The Gondwana Assembly 520-450 Ma, and Gondwana breakup 140-130 Ma.

The assembly of Gondwanaland lasted from c720-500 Ma; and in addition to Wegener's Pangea (c. 325-175 Ma). Older supercontinents that existed before Pangea was based on 'common' isotopic ages observed in various places around the globe. The ages obtained from the study area were plotted on the age time chart to depict the evolution of the area with opening and closing events ranging from Nuna-Columbia (Mirgarani Granite) to Rodinia and Pangea-Amasia (**Figure 18c**, and **Table 7**). Dudhi group granitic intrusions between 1.9 to 1.7 Ga are accretion orogen during Columbia-Nuna, igneous activities between 1100 to 700 Ma are correlated with Rodinia, and no igneous activities were observed during the Cryogenian period ca. 720-635 Ma, however, the Gondwana sedimentation took place in the grabens in CGGC. Alkaline and acidic magmatism was again seen during 435 to 117-113 Ma Pan African activities related to Pangea breakup and continent movement due to Kerguelen plume activity [116].

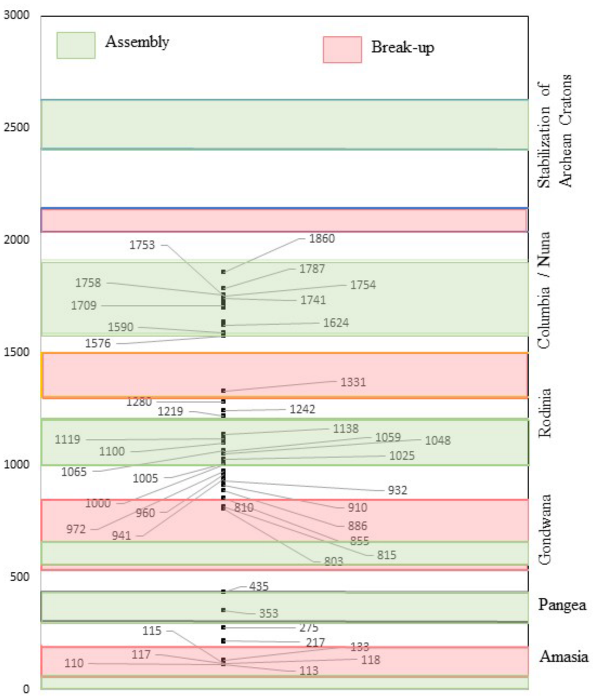

Figure 18c. Supercontinents assembly, break-ups, and relationships of various intrusive and extrusive phases in CGGC.

13. Conclusions

The Mirgarani pluton was emplaced at 1636 ± 66 Ma. It emplaced into the collisional compressional environment between the late Paleo- to early Mesoproterozoic. Geochemically Mirgarani granite is subalkalic peraluminous high silica, iron, potassic, low calcic, and magnesium-bearing S-type granite. It is corundum normative and garnet's presence further corroborates its S-Type characteristics. It is enriched in K_2O, FeO, Rb, Pb, Th, U, Cr, Ni, and Co and depleted in Sr, Nb, Ba, and Zr as compared to the normal granite. Mirgarani granite is formed due to the partial melting or crystal fraction during the granitization of clay-rich metagraywacke. The temperature of magma was ranging between 764-837 °C with an average of 789 °C. It's due to elevated Zircon concentration varying from 104-247 ppm with an average of 143 ppm. It has elevated contents of U, Th, and K resulting in its high heat capacity of 2.38 to 22.78 $mW \cdot m^{-3}$ with an average of 10.90 $mW \cdot m^{-3}$. The Dudhi group of rocks has high heat-producing capacities. It is related to compressional environment during the Columbian - Nuna supercontinent. The review of geochronological data especially from the Northwestern and Western parts of CGGC shows five phases of tectono-magmatic activities viz. Phase I 1880 to 1000 Ma, Phase II 980 to 880 Ma, Phase III 435-353 Ma, Phase IV 275-214 Ma, and Phase V 185-100 Ma. The alkaline magmatism and the igneous activities ranges from the Columbian (Nuna) to Rodinia and Gondwanaland/Pannotia.

Conflicts of Interest

The author declares no conflicts of interest regarding the publication of this paper.

Acknowledgement

The author is grateful to the Atomic Minerals Directorate for Exploration and Research (AMD), and the Department of Atomic Energy (DAE) for providing logistics for field investigations AMD XRF lab is acknowledged for analytical support.

References

[1] Dayal, B., 1979. A conceptual approach for the possibility of Tin mineralisation associated with acid magmatism in parts of Mirzapur district Uttar Pradesh Proc. workshop (IGCP-26) in Mineralisation associated with acid magmatism (MAWAM 1979). Geological Survey of India. 13, 111-116.

[2] Iqabaluddin, Moghani, A., 1981. Stratigraphy of the Bijawar Group in Sun Valley, Mirzapur district, UP and Sidhi district, MP. Geological Survey of India. 3, 81-93.

[3] Chaubey, V.D., Gupta, A., 1990. The Son-valley greenstone belt-some aspects of Precambrian shield geology, Peninsular India. Journal of the Geological Society of India. 35, 229-305.

[4] Nair, K.K.K., Jain, S.C., Yedekar, D.B., 1995. Stratigraphy Structure and Geochemistry of the Mahakoshal Greenstone belt. Memoir Geological Society of India. 31, 403-432.

[5] Yadav, N.L., 1978. Petrochemistry of Pre-Cambrian rocks of Dudhi area, District Mirzapur UP in Recent research in Geology. Hindustan Publication Corporation: Delhi. pp. 447-465.

[6] Bhattacharya, A.K., Gorikhan, R.A., Khajanchi, B.N., et al., 1992. Uranium mineralization hosted by migmatite-mobilizates and breccia zones in the northwestern part of Chhotanagpur granite gneiss complex, Rihand valley, Sonbhadra district Uttar Pradesh. Indian Journal of Geology. 64(3), 259-275.

[7] Mahadevan, T., 2002. Geology of Bihar and Jharkhand. GSI Publications. 2(1).

[8] Acharyya, S.K., 2003. The nature of mesoproterozoic central Indian tectonic zone with exhumed and reworked older granulites. Gondwana Research. 6, 197-214.

[9] Sarkar, S.N., 1980. Precambrian stratigraphy and geochronology of Peninsular India: A review. Indian Journal of Earth Sciences. 7, 12-26.

[10] Sarkar, A.N., 1982. Precambrian tectonic evolution of Eastern India: A model of converging microplates. Tectonophysics. 86, 363-397.

[11] Sarkar, A.N., 1988. Tectonic evolution of the Chotanagpur Plateau and the Gondwana Basins in Eastern India: An interpretation based on supra-subduction geological processes. Mukhopadhaya, D. (editor), precambrian of the Eastern Indian shield. Geological Society of India Memoir. 8, 127-148.

[12] Chatterjee, N., Banerjee, M., Bhattacharya, A., et al., 2010. Monazite chronology, metamorphism–anatexis and tectonic relevance of the mid-Neoproterozoic Eastern Indian Tectonic Zone. Precambrian Research. 179, 99-120.
DOI: https://doi.org/10.1016/j.precamres.2010.02.013

[13] Chatterjee, N., Ghose, N.C., 2011. Extensive early neoproterozoic high-grade metamorphism in North chotanagpur gneissic complex of the central Indian Tectonic Zone. Gondwana Research. 20(2-3), 362-379.
DOI: https://doi.org/10.1016/j.gr.2010.12.003

[14] Mohanty, S., 2012. Spatio-temporal evolution of the Satpura Mountain Belt of India: A comparison with the Capricorn Orogen of Western Australia and implication for evolution of the supercontinent Columbia. Geoscience Frontiers. 3(3), 241-267.
DOI: https://doi.org/10.1016/j.gsf.2011.10.005

[15] Sanyal, S., Sengupta, P., 2012. Metamorphic evolution of the Chotanagpur Granite Gneiss Complex of the East Indian Shield: Current status. Geological Society, London, Special Publications. 365(1), 117-145.
DOI: https://doi.org/10.1144/sp365.7

[16] Mukherjee, S., Dey, A., Sanyal, S., et al., 2019. Proterozoic crustal evolution of the Chhotanagpur granite gneissic complex, Jharkhand-Bihar-West Bengal, India: Current status and future prospect tectonics and structural geology in Indian Context Soumyajit Mukherjee (editor). Springer International Publication: New York. pp. 7-54.

[17] Auden, J.B., 1933. Vindhyan sedimentation in the sun valley, Mirzapur district. Geological Survey of India. 62(2), 141-250.

[18] Chaubey, V.D., 1970. The Narmada-Son line thrust, the great boundary fault along the southern margin of Vindhyan basin, Central India, West Commemoration volume. Today and Tomorrow's Printers and Publishers, Faridabad: Delhi. pp. 420-438.

[19] Gupta, A., 1982. Interpretation of Landsat imagery of a part of the Son Valley and its correlation with Bouguer gravity and airborne magnetic anomaly data. Journal of the Geological Society of India. 23, 136-145.

[20] Dhurandhar, A.P., Saxena, D.N., 1996. Integrated airborne gamma-ray spectral and satellite data analysis for U and REE mineralisation-A case study from north Sagobandh area, District Sonbhadra, Uttar Pradesh, India. Journal of the Indian Society of Remote Sensing. 27(1), 43-57.
DOI: https://doi.org/10.1007/bf02990774

[21] Dhurandhar, A.P., Rajagopalan, V., Raminaidu, Ch.,

et al., 2003. Petrological and geochemical characterisation of uraniferous pegmatoid leucosomes of Jura, District Sonbhadra, Uttar Pradesh, India. Gond. Geol. Magz. SPL. 7, 279-295.

[22] Dhurandhar, A.P., Latha, A., Krishna, V., 2005. Geochronology and Petrochemistry of the Dubha Granite, Sonbhadra District, Uttar Pradesh. Journal of the Geological Society of India. 65(4), 459-467.

[23] Dhurandhar, A.P., Srivastava, S.K., Sastry, D.V.L.N., et al., 2006. Geochemistry and geochronology of metabasic intrusions in Kirwil-Sagobandh Area, North-western Chhotanagpur Terrain. Indian Journal of Petroleum Geology. 78(1-4), 119-134.

[24] Hansoti, S.K., Deshmukh, A.N., 1990. Structural controls of uranium mineralisation in Proterozoic rocks of Sendur Tatapani area, Sarguja district MadhyaPradesh. Precambians of Central India. Geological Survey of India Special Publication. 28, 676-695.

[25] Streckiessens, A., 1976. To each plutonic rock its proper name. Earth Science Reviews. 12, 1-33.

[26] Ludwing, K.R., 2012. ISOPLOT 3.75 A Geochronological Toolkit for Microsoft Excel. Berkeley Geochronology Center Special Publication. 5, 75.

[27] Pandey, B.K., Gupta, J.N., Sarma, K.J., et al., 1997. Sm-Nd, Pb-Pb, and Rb-Sr geochronology and petrogenesis of mafic dyke swarm of Mahbubnagar, south India: Implications for Paleoproterozoic crustal evolution of the eastern Dharwar craton. Precambrian Research. 84, 181-196.

[28] Wedepohl, K.H., 1969. Handbook of geochemistry. New York: Springer-Verlog. 1, 236.

[29] Gao, S., Luo, T.C., Zhang, B.R., et al., 1998. Chemical composition of the continental crust as revealed by studies in east China. Geochimica et Cosmochimica Acta. 62, 1959-1975.

[30] Thompson, R.N., 1982. Magmatism of the British Tertiary Volcanic Province. Scottish Journal of Geology. 18(1), 49-107. doi: 10.1144/sjg18010049.

[31] McDonough, W.F., Sun, S.S., 1995. The composition of the Earth. Chemical Geology. 120, 223-253.

[32] Maniar, P.D., Piccoli, P.M., 1989. Tectonic discrimination of granitoids. Geological Society of America Bulletin. 101, 635-643.

[33] Cox, K.G., Bell, J.D., Pankhurst, R.J., 1979. The interpretation of igneous rocks. Allen and Unwin: London. pp. 450.
DOI: https://doi.org/10.1007/978-94-017-3373-1

[34] Patiño Douce, A.E., 1999. What do experiments tell us about the relative contributions of crust and mantle to the origin of granitic magmas? Castro, A., Fernandez, C., Vigneresse, J. L. (editors), Understanding Granites: Integrating New and Classical Techniques. Geological Society, London, Special Publications. 168, 55-75.

[35] Condie, K.C., 1973. Archean magmatism and crustal thickening. Geological Society of America Bulletin. 84, 2981-2991.
DOI: https://doi.org/10.1130/0016-7606(1973)84<2981:AMACT>2.0.CO;2

[36] Wilson, M., 1989. Igneous petrogenesis a global tectonic approach. London: Unwin Hyman. pp. 126, 466.

[37] Jung, C., Jung, S., Hellebrand, E., et al., 2009. Trace element constraints on mid-crustal partial melting processes—a garnet ion probe study from polyphase migmatites (Damara orogen, Namibia). Transactions of the Royal Society of Edinburgh Earth Sciences. 100(1-2), 205-218.

[38] Chappell, B.W., White, A.J.R., 1974. Two contrasting granite types. Pacific Geology. 8, 173-174.

[39] Chappell, B.W., White, A.J.R., 2001. Two contrasting granite types: 25 years later. Australian Journal of Earth Sciences. 48, 489-499.

[40] White, A.J.R., Chappell, B.W., 1977. Ultrametamorphism and granitoid genesis. Tectonophysics. 43(1-2), 7-22.
DOI: https://doi.org/10.1016/0040-1951(77)90003-8

[41] White, A.J.R., Chappell, B.W., 1983. Granitoid types and their distribution in the Lachlan Fold Belt, southeast Australia. Roddick, J.A., (editor), Circum-Pacific Plutonic terranes. Geological Society of America, Memoir. 159, 21-34.
DOI: https://doi.org/10.1130/MEM159-p21

[42] White, A.J.R., Chappell, B.W., 1988. Some supracrustal (S-type) granites of the Lachlan Fold Belt. Transactions of the Royal Society of Edinburgh. Earth Sciences. 79, 169-181.

[43] Calvin, F.M., 1985. Are strongly peraluminous magmas derived from pelitic sedimentary sources? Journal of Geology. 93, 673-689.

[44] El Bouseily, A.M., El Sokkary, A.A., 1975. The relation of Rb, Ba, and Sr in granitic rocks. Chemical Geology. 16, 207-219.

[45] Streckeisen, A.L., LeMaitre, R.W., 1979. Chemical approximation to modal QAPF classification of the igneous rocks. Neus Jahrbuch fur Mineralogie. 136, 169-206.

[46] Shaw, D.M., 1968. A review of K-Rb fractionation trends by covariance analysis. Geochimica Et Cosmochimica Acta. 32, 573-601.

[47] Rossi, J.N., Toselli, A.J., Basei, M.A., et al., 2011. Geochemical indicators of metalliferous fertility in the Carboniferous San Blas pluton, Sierra de Velasco, Argentina. Geological Society, London, Special Publications. 350(1), 175-186.
DOI: https://doi.org/10.1144/sp350.1010.1144/sp350.10
[48] Clarke, D.B., 1992. The mineralogy of peraluminous granites: A review. Canadian Mineralogist. 19, 3-17.
[49] Rollinson, H.R., 1993. Using geochemical data: Evaluation, presentation, interpretation. 1st edition. Longman: London. pp. 384.
[50] Janoušek, V., Finger, F., Roberts, M.P., et al., 2004. Deciphering petrogenesis of deeply buried granites: Whole-rock geochemical constraints on the origin of largely undepleted felsic granulites from the Moldanubian Zone of the Bohemian Massif. Earth & Environmental Science Transactions of the Royal Society of Edinburgh. 95, 141-159.
DOI: https://doi.org/10.1017/S0263593300000985
[51] Sylvester, P.J., 1998. Post-Collisional strongly peraluminous granites. Lithos. 45(1-4), 29-44.
[52] Dietrich, V., Gansser, A., 1981. The leucogranites of the Bhutan Himalaya. Schweizer Mineralogisch Petrographische Mitteilungen. 61, 177-202.
[53] Visona, D., Lombardo, B., 2002. Two-mica and tourmaline leucogra-718nites from the Everest-Makalu region (Nepal-Tibet). Himalayan719leucogranite genesis by isobaric heating? Lithos. 62, 125-150.
[54] Watson, E.B., Harrison, T.M., 1983. Zircon saturation revisited: Temperature and composition effects in a variety of crustal magma types. Earth and Planetary Science Letters. 64, 295-304.
DOI: https://doi.org/10.1016/0012-821X(83)90211-X
[55] Watson, E.B., Harrison, T.M., 1984. Accessory phases and the geochemical evolution of crustal magmas. Physics of the Earth and Planetary Interiors. 35, 19-30.
DOI: https://doi.org/10.1016/0031-9201(84)90031-1
[56] Winkler, H.G.F., 1974. Petrogenesis of metamorphic rocks. Springer-Verlag: New York. pp. 320.
[57] James, R.S., Hamilton, D.L., 1969. Phase relation in the system $NaAlSi_3O_8$-$KAlSi_3O_8$-$CaAl_2Si_2O_8$ at 1-kilobar water vapour pressure. Contributions to Mineralogy & Petrology. 21, 111-141.
[58] Wollenberg, H.A., Smit, A.R., 1987. Radiogenic heat production of crustal rocks: an assessment based on geochemical data. Geophysical Research Letters. 14(3), 295-298.
[59] Artemieva, I.M., Thybo, H., Jakobsen, K., et al., 2017. Heat production in granitic rocks: Global analysis based on a new data compilation. GRANITE2017, Earth-Science Reviews. 172, 1-26.
[60] Pearce, J.A., Nigel, B.W.H., Andrew, G.T., 1984. Trace element discrimination diagrams for the tectonic interpretation of granitic rocks. Journal of Petrology. 25, 956-983.
[61] Ghose, N.C., 1992. Chhotanagpur gneiss-granulite complex, eastern India: Present status and future prospect. Indian Journal of Geology. 64(1), 100-121.
[62] Emslie, R.F., 1978. Anorthosite massif, Rapakivi granites and late Proterozoic rifting od North America. Precambrian Research. 7, 61-98.
[63] Dewey, J.F., Bruke, K.C.A., 1973. Tibetian, Variscan and Precambrian basement reactivation products of continental collision. Journal of Geology. 81, 683-692.
[64] Gupta, J.N., Pandey, B.K., Prasad, R.N., et al., 1988. Rb-Sr geochronology of some granitic rocks around Arbail and age of uraniferous aerinite and quartz pebble conglomerates of western Karnataka. Geological Society of India Memoir. 9, 101-108.
[65] Armstrong, R.L., 1968. A model for the evolution of strontium and lead isotopes in a dynamic earth. Reviews of Geophysics. 6(2), 175-199.
[66] Patterson, C., Tatsumoto, M., 1964. The significance of lead isotopes in detrital feldspar with respect to chemical differentiation within the earth's mantle. Geochimica et Cosmochimica Acta. 28, 1-22.
[67] Stueber, A.M., Ramamurthy, V., 1966. Strontium isotope and alkali element abundances in ultramafic rocks. Geochimica et Cosmochimica Acta. 28, 1243-1259.
[68] Faure, G., Hurley, P.M., 1963. The isotopic composition of strontium in oceanic and continental basalts: Application to the origin of igneous rocks. Journal of Petrology. 4, 31-50.
[69] Hurley, P.M., Hughes, H., Faure, G., et al., 1962. Radiogenic strontium-87 model of continent formation. Journal of Geophysical Research. 67, 5316.
[70] Davies, R.D., Allsopp, H.L., Erlank, A.J., et al., 1970. Sr-isotopic studies on various layered intrusions in southern Africa. Special Publication of the Geological Society of South Africa. 1, 576-593.
[71] Moorbath, S., 1975. Evolution of Precambrian crust from strontium isotopic evidences. Nature. 254, 395-398.
[72] Holmes, A., Leland, W.T., Nier, A.O., 1950. Age of uranite from a pegmatite near Singar Gaya district.

India American Mineralogist. 35(1-2), 19-28.
[73] Holmes, A., 1955. Dating the Precambrian of peninsular India and Cylon. Geological Association of Canada. 7, 81-106.
[74] Mandal, P., 2016. Shear-wave splitting in Eastern Indian Shield: Detection of a Pan-African suture separating Archean and Meso-Proterozoic terrains. Precambrian Research. 275, 278-285.
DOI: https://doi.org/10.1016/j.precamres.2016.01.019
[75] Pandey, B.K., Chabria, T., Gupta, J.N., 1995. Geochronological characterisation of the proterozoic terrains of peninsular India: Relevance to the first-order target selection for uranium exploration. Exploration & Research for Atomic Minerals. 8, 187-213.
[76] Pandey, D., Sinha, K.K., Sharma, P.K., 2004. Jhirgadandi Pluton—A Lower Proterozoic, A-Type, Anorogenic, Within—Plate Granite from the son-Narmada Lineament, Sonbhadra district, Uttar Pradesh. Precambrian Crustal Evolution and Metallogenesis with Special Reference to Central India. Hindustan Publishing Corporation (India): New Delhi.
[77] Sastry, D.V.L.N., Krishna, V., Latha, A. (editors), et al., 2017. Rb-Sr and Pb-Pb geochronological studies on the granites of Jaurahi Sonbhadra District UP. National Symposium on Emerging Trends in Geosciences, Mineral Exploration, and Environmental Sciences for Sustainable Developments; 2017 Dec 20-21; Hyderabad, India. India: Indian society of Applied geochemists and Atomic Minerals Directorate for Exploration and Research. p. 49-50.
[78] Sarkar, A., Bodas, M., Kundu, H.K. (editors), et al., 1998. Geochronology and geochemistry of Mesoproterozoic intrusive plutonites from the eastern segment of the Mahakoshal green stone belt, central India. Proceedings of International Seminar on "Precambrian crust in eastern and central India"; Bhubaneswar. p. 82-85.
[79] Pandey, B.K., Krishna, V., Chabria, T. (editors), 1998. An overview of the geochronological data on the rocks of Chhotanagpur gneiss-granulite complex and adjoining sedimentary sequences, Eastern and Central India. Abstract Volume, International Seminar on "Precambrian crust in eastern and central India"; Bhubaneswar. pp. 131-135.
[80] Ray Barman, T., Bishui, P.K., Mukhopadhyay, K., et al., 1994. Rb-Sr geochronology of the high-grade rocks from Purulia, West Bengal, and Jamua-Dumka sector, Bihar. Indian Minerals. 48, 45-60.
[81] Karmakar, S., Bose, S., Sarbadhikari, A.B., et al., 2011. Evolution of granulite enclaves and associated gneisses from Purulia, Chhotanagpur Granite Gneiss Complex, India: Evidence for 990-940Ma tectonothermal event(s) at the eastern India cratonic fringe zone. Journal of Asian Earth Sciences. 41(1), 69-88.
DOI: https://doi.org/10.1016/j.jseaes.2010.12.006
[82] Jain, S.C., Nair, K.K.K., Yedekar, D.B., 1995. Tectonic evolution of the Son-Narmada-Tapti Lineament zone in Geoscientific studies of Son-Narmada-Tapti Lineament zone, Project CRUMENSONATA. Geological Survey of India. 10, 333-371.
[83] Bora, S., Kumar, S., Yi, K., et al., 2013. Geochemistry and U-Pb SHRIMP zircon chronology of granitoids and microgranular enclaves from Jhirgadandi Pluton of Mahakoshal Belt, Central India Tectonic Zone, India. Journal of Asian Earth Sciences. 70-71, 99-114.
[84] Bora, S., Kumar, S., 2015. Geochemistry of biotites and host granitoid plutons from the Proterozoic Mahakoshal Belt, central India Tectonic Zone: Implication for nature and tectonic setting of magmatism. International Geology Review. 57(11-12), 1686-1706.
DOI: https://doi.org/10.1080/00206814.2015.1032372
[85] Mallik, A.K., Gupta, S.N., Ray Barman, T., 1991. Dating of early Precambrian granite–greenstone complex of the Eastern Indian Precambrian shield with special reference to the Chotanagpur granite gneiss complex. Records of the Geological Survey of India. 124, 20-21.
[86] Pandey, B.K., Gupta, J.N., Lal, Y., 1986. Whole rock and mineral isochron ages for the granites from Bihar Mica Belt of Hazaribagh Bihar, India. Indian Journal of Earth Sciences. 12(2&3), 157-162.
[87] Pandey B.K., Upadhyady, L., Sinha, K.K., 1986. Geochronology of Jajawal-Binda-Nagnaha granitoids in relation to uranium mineralization. Indian Journal of Earth Sciences. 12(2&3), 163-168.
[88] Vinogradov, A., Tugarinov, A., Zhykov, C., et al., 1964. Geochronology of Indian Precambrian, 22nd Session of the International Geological Congress. X, 553-567.
[89] Holmes, A., Leland, W.T., Nier, A.O., 1950. Age of uranite from a pegmatite near Singar Gaya district. India American Mineralogist. 35(1-2), 19-28.
[90] Nandi, S.K., Sen, D.N., 1950. Investigation on Indian radioactive minerals, II, Allanite. Journal of

Vacuum Science & Technology. 9, 124-128.

[91] Sarkar, T.C., 1941. The lead ratio of a crystal of monazite from the Gaya district Bihar, India. Proceedings of the Indian Academy of Sciences Section A. 13, 245-248.

[92] Krishnan, M.S., 1953. Structural and tectonic history of India. Geological Survey Memoir. 81, 1-93.

[93] Krishna, V., Sastry, D.V.L.N., Pandey, B.K. (editors), et al., 2003. U-Pb and Pb-Pb ages on columbite-tantalite minerals from pegmatites of Bihar Mica Belt, Jharkhand, India. Silver Jubilee Symp., Nat. Inst. Oceanography, Goa. India: Indian Soc. Mass Spec. p. 650-653.

[94] Lal, N., Saini, H.S., Nagpaul, K.K., et al., 1976. Tectonic and cooling history of the Bihar Mica Belt, India, as revealed by fission-track analysis. Tectonophysics. 34(3-4), 163-180.

DOI: https://doi.org/10.1016/0040-1951(76)90094-9

[95] Aswathanarayana, U., 1956. Absolute ages of the Archaean orogenic cycles of India. American Journal of Science. 254(1), 19-31.

DOI: https://doi.org/10.2475/ajs.254.1.19

[96] Baidya, T.K., Chakravarthy, P.S., 1988. Mineralisation in Belamu-Jaipur sector of northwestern Purulia district, West Bengal. Memoir-Geological Society of India. 8, 147-165.

[97] Singh, Y., Krishna, V., 2009. Rb-Sr geochronology and petrogenesis of granitoids from the chhotanagpur granite gneiss complex of Raikera-Kunkuri Region, Central India. Journal of the Geological Society of India. 74, 200-208.

[98] Ghose, N.C., Smakin, B.M., Smirnov, V.N., 1973. Some geochronological observations on the precambrians of Chhotangpur Bihar, India. Geological Magazine. 110, 477-482.

[99] Sarkar, A. (editor), 1974. K-Ar age of Mahuadanr rhyodacite: Evidence for late Triassic effusive activity in Eastern India. 9th International Gondwana Symposium, Hyderabad. p. 687-695.

[100] Sarkar, A., Paul, D.K., Balasubrahmanyan, M.N., et al., 1980. Lamprophyres from the Indian Gondwanas—K–Ar ages and chemistry. Journal Geological Society India. 21, 188-193.

[101] Baksi, A.K., 1995. Petrogenesis and timing of volcanism in the Rajmahal flood basalt province, northeastern India. Chemical Geology. 121(1-4), 73-90.

DOI: https://doi.org/10.1016/0009-2541(94)00124-q

[102] Sarkar, A., Datta, A.K., Poddar, B.C., et al., 1996. Geochronological studies of Mesozoic igneous rocks of eastern India. Journal of Southeast Asian Earth sciences. 13, 77-81.

[103] Eriksson, P.G., Mazumder, R., Catuneanu, O., et al., 2006. Precambrian continental freeboard and geological evolution: A time perspective. Earth-Science Reviews. 79, 165-204.

[104] Lubnina, N.V., Slabunov, A.I., 2011. Reconstruction of the Kenorland supercontinent in the Neoarchean based on paleomagnetic and geological data. Moscow University Geology Bulletin. 66, 242-249.

DOI: https://doi.org/10.3103/S0145875211040077

[105] Mints, M.V., Eriksson, P.G., 2016. Secular changes in relationships between plate-tectonic and mantle-plume engendered processes during Precambrian time. Geodynamics & Tectonophysics. 7(2), 173-232.

DOI: https://doi.org/10.5800/GT-2016-7-2-0203

[106] Zhang, S., Zheng, X.L., Evans, D.A.D., et al., 2012. Pre-Rodinia supercontinent Nuna shaping up: A global synthesis with new paleomagnetic results from North China. Earth and Planetary Science Letters. 353-354, 145-155.

[107] Nance, D.R., Murphy, B.J., 2013. Origins of the supercontinent cycle. Geoscience Frontiers. 4(4), 439-448.

DOI: https://doi.org/10.1016/j.gsf.2012.12.007

[108] Meert, J.G., Santhosh, M., 2017. The Columbia supercontinent revisited. Gondwana Research. 50, 67-83.

[109] Evans, D.A.D., Mitchell, R.N., 2011. Assembly and breakup of the core of Paleoproterozoic—Mesoproterozoic supercontinent Nuna. Geology. 39(5), 443-446.

DOI: https://doi.org/10.1130/G31654.1

[110] Li, Z.X., Bogdanova, S.V., Collins, A.S., et al., 2008. Assembly, configuration, and break-up history of Rodinia-A synthesis. Precambrian Research. 160(1-2), 179-210.

DOI: https://doi.org/10.1016/j.precamres.2007.04.021

[111] Long, J., Zhang, S., Luo, K., 2019. Cryogenian magmatic activity and early life evolution. Scientific Reports. 9(1).

DOI: https://doi.org/10.1038/s41598-019-43177-8

[112] Dalziel, I.W.D., 1997. Neoproterozoic-Paleozoic Geography and Tectonics: Review, hypothesis, environmental speculation. Geological Society of America Bulletin. 109, 16-42.

DOI: https://doi.org/10.1130/0016-7606(1997)109<0016:ONPGAT>2.3.CO;2

[113] Dalziel, I.W.D., 2013. Antarctica and supercon-

tinental evolution: Clues and puzzles. Earth and Environmental Science Transactions of the Royal Society of Edinburgh. 104, 3-16.
DOI: https://doi.org/10.1017/S1755691012000096

[114] Unrug, R., 2007. Rodinia to Gondwana: The geodynamic map of Gondwana supercontinent assembly. GSA Today. 7(1), 2-6.

[115] Nance, R.D., Murphy, J.B., 2018. Supercontinents and the case for Pannotia. Wilson, R.W., Houseman, G.A., Mccaffrey, K.J.W., Doré, A.G., Buiter, SJH (editors). Fifty Years of The Wilson Cycle Concept in Plate Tectonics. 470, 1-17.
DOI: https://doi.org/10.1144/ SP470.5

[116] Kent, R.W., Storey, M., Saunders, A.D., 1992. Large igneous provinces: Sites of plume impact or plume incubation. Geology. 20, 891-894.